

Extracting the mass scale of a second Higgs boson from a deviation in $h(125)$ couplings

Simone Blasi,^{1,*} Stefania De Curtis,^{1,†} and Kei Yagyu^{1,‡}

¹*INFN, Sezione di Firenze, and Department of Physics and Astronomy,
University of Florence, Via G. Sansone 1, 50019 Sesto Fiorentino, Italy*

We investigate the correlation between a possible deviation in the discovered Higgs boson $h(125)$ couplings from the Standard Model prediction and the mass scale ($M_{2\text{nd}}$) of the next-to-lightest Higgs boson in models with non-minimal Higgs sectors. In particular, we comprehensively study a class of next-to-minimal Higgs sectors which satisfy the electroweak ρ parameter to be one at tree level. We derive an upper limit on $M_{2\text{nd}}$ by imposing bounds from perturbative unitarity, vacuum stability, triviality and electroweak precision data as functions of the deviation in the hVV ($V = W, Z$) couplings. Furthermore, we discuss the complementarity between these bounds and the current LHC data, e.g., by considering direct searches for additional Higgs bosons and indirect constraints arising from the measured $h(125)$ signal strengths.

*Electronic address: simone.blasi.91@gmail.com

†Electronic address: decurtis@fi.infn.it

‡Electronic address: yagyu@fi.infn.it

I. INTRODUCTION

The existence of at least one isospin doublet scalar field is strongly suggested by the discovery of the Higgs boson $h(125)$ at the LHC and the measurement of its properties, which are consistent with those of the Standard Model (SM) Higgs boson [1]. This experimental fact brings us to the natural question whether the observed Higgs boson is unique or it corresponds to one of the resonances of a wider structure. The latter possibility requires the Higgs sector to be extended from the minimal form. On the other hand, a non-minimal shape of the Higgs sector is expected by New Physics (NP) paradigms (e.g., composite Higgs models and supersymmetry) embedded in physics beyond the SM (BSM). Therefore, the detection of a second Higgs boson would be a clear evidence of NP.

The mass of a Higgs boson is one of the most critical parameters for its direct detection at collider experiments. In this paper, we aim to systematically derive the limits on the mass of a second Higgs boson in next-to-minimal renormalizable Higgs sectors, i.e., those composed of one isospin doublet plus an extra Higgs field with a non-vanishing Vacuum Expectation Value (VEV). If we require the VEV of the extra Higgs field not to spoil the relation for the electroweak parameter $\rho = 1$ at tree level, the simplest three choices are: the Higgs Singlet Model (HSM), the 2 Higgs Doublet Model (2HDM) [2] and the Georgi-Machacek (GM) model [3, 4]¹. These extensions, which are commonly understood as low energy descriptions of underlying NP scenarios, have been largely considered in the literature because of their connection with several open questions of the SM. It is known that the HSM can provide a candidate for dark matter [5], while models with Higgs triplets are involved in generating neutrino masses through the so-called type II seesaw mechanism [6]. Conversely, the interest in 2HDMs is mainly motivated by supersymmetric extensions of the SM. Furthermore, the reason to consider models with an extended Higgs sector is phenomenological. As mentioned above, the discovery of a second Higgs boson would necessarily require to build-up a non-minimal structure for the Higgs sector. In addition, non-minimal Higgs sectors can be indirectly probed by precise measurements of the h couplings to SM particles, because the h state is there generally realized through a non-zero mixing among all the other scalars with

¹ In fact, although the Higgs sector of the GM model is composed of one iso-doublet and two iso-triplet scalar fields, the latter can be packaged as one $SU(2)_L \times SU(2)_R$ bi-triplet. We thus regard the GM model as the next-to-minimal Higgs sector containing triplets.

the same quantum numbers, resulting deviations in the h couplings from the SM prediction. Regarding, e.g., the coupling to a vector boson pair, the current 1σ uncertainty at the LHC is indeed about 10% [1], so that there is still room for a sensible NP contribution. Such uncertainty is expected to be reduced to $\sim 5\%$ by the forthcoming LHC High Luminosity option [7, 8] and even to 0.5% at future e^+e^- colliders [9].

Basically, the masses of extra Higgs bosons within a given model are free parameters. However, it is possible to extract their order of magnitude by taking into account theoretical issues within particular BSM scenarios. For example, it is known that perturbative unitarity constrains the size of dimensionless quartic couplings in the Higgs potential which actually enter the expression of the physical Higgs boson masses. Originally, this method was applied to set an upper limit on the SM Higgs boson mass by Lee, Quigg and Thacker [10]. Afterwards, the same technique was carried out in various extended Higgs sectors such as 2HDMs [11–14]. Besides that, the reliability of a perturbative approach requires the scalar potential to be bounded from below in any direction of the field space. Such requirement is usually referred to as vacuum stability and it provides further constraints on the parameter space of non-minimal Higgs sectors. Furthermore, one requires the absence of Landau poles up to a certain cutoff of a given model: this is the so-called triviality constraint.

Bounds on the mass of extra Higgs bosons can be extracted by considering experimental issues as well. We here take into account the constraints coming from the Electroweak Precision Tests (EWPTs) and the currently available LHC data, which are based both on the null excess of signatures from direct searches for extra Higgs bosons and on the analysis of the $h(125)$ signal strengths. Combining both theoretical and experimental requirements, we restrict the possible allowed values of the extra Higgs masses, depending on the model and its parameter configurations.

It is useful for this analysis to discuss the decoupling and the alignment limits of non-minimal Higgs sectors. The decoupling limit is defined in such a way that all the masses of the extra Higgs bosons are taken to infinity, and eventually only the h state remains light. In this limit, the extended Higgs sectors effectively reduce to the minimal one and all the observables relevant to h , such as the couplings to SM particles, do not deviate from the SM prediction. On the other hand, the alignment limit is defined such that the h state and the Nambu-Goldstone (NG) bosons emerging from the electroweak spontaneous symmetry breaking fill the same doublet field, which carries the whole VEV v , fixed by $v = (\sqrt{2}G_F)^{-1/2}$,

Model	Scalar fields $\sim (SU(2)_L, U(1)_Y)$
HSM	$\Phi(\mathbf{2}, 1/2)$ and $S(\mathbf{1}, 0)$
2HDM	$\Phi_1(\mathbf{2}, 1/2)$ and $\Phi_2(\mathbf{2}, 1/2)$
GM model	$\Phi(\mathbf{2}, 1/2)$, $\xi(\mathbf{3}, 0)$ and $\chi(\mathbf{3}, 1)$

TABLE I: Electroweak quantum numbers of the scalar fields in the non-minimal Higgs sectors considered.

with G_F being the Fermi constant. In this limit, all the h couplings to SM particles such as hVV ($V = W^\pm, Z$) and hff align to be the same as their SM values at tree level. Notice that the decoupling limit can only be taken if the alignment limit is realized. Therefore, a deviation from the alignment limit, which gives a non-zero deviation in h couplings from the SM prediction, results in an upper bound on the extra Higgs boson masses. In particular, we investigate the correlation between a deviation in the h coupling to a vector boson pair and the bounds on the extra Higgs boson masses by taking into account the aforementioned constraints for each extended Higgs sector.

This paper is organized as follows. In Sec. II, we define the three models with non-minimal Higgs sectors, i.e., the HSM, the 2HDM and the GM model. In Sec. III, we numerically extract, for each model, the upper limit on the mass of the next-to-lightest Higgs boson by imposing the theoretical constraints (unitarity, vacuum stability, triviality) and those coming from the EWPTs. In Sec. IV, the complementarity between the bounds from the LHC data and those of Sec. III is studied. Our conclusions are summarized in Sec. V.

II. EXTENDED HIGGS SECTORS

We briefly review the three extended Higgs models considered in this paper, namely, the HSM, the 2HDM and the GM model. The scalar field content is summarized in Table I. Throughout the paper, we use the shorthand notation: $s_X = \sin X$, $c_X = \cos X$ and $t_X = \tan X$ for an arbitrary angle parameter X . In each model, the symbol h is used to denote the discovered Higgs boson at the LHC with a mass of 125 GeV ($m_h = 125$ GeV).

A. Higgs Singlet Model

The most general scalar potential in the HSM has the following form:

$$V(\Phi, S)_{\text{HSM}} = \mu^2 |\Phi|^2 + \lambda |\Phi|^4 + \mu_{\Phi S} |\Phi|^2 S + \lambda_{\Phi S} |\Phi|^2 S^2 + t_S S + m_S^2 S^2 + \mu_S S^3 + \lambda_S S^4, \quad (1)$$

where the doublet and the singlet fields are respectively parameterized as

$$\Phi = \begin{pmatrix} G^+ \\ \frac{\phi + v + iG^0}{\sqrt{2}} \end{pmatrix}, \quad S = v_S + s. \quad (2)$$

In Eq. (2), G^\pm and G^0 are the NG bosons which are absorbed by the longitudinal components of the W^\pm and Z bosons, respectively. The VEV of the singlet field v_S contributes neither to the electroweak symmetry breaking nor to the fermion mass generation. As a consequence, we can set $v_S = 0$ without loss of generality because of the shift symmetry of the singlet VEV [15, 16], and we will adopt it throughout this paper.

From the tadpole conditions

$$\left. \frac{\partial V}{\partial \phi} \right|_0 = \left. \frac{\partial V}{\partial s} \right|_0 = 0, \quad (3)$$

we can eliminate t_S and μ^2 parameters. In Eq. (3) and in the following, the symbol $|_0$ denotes that all the scalar fields are taken to be zero after the derivative. The mass eigenstates for the neutral Higgs bosons can be defined as

$$\begin{pmatrix} s \\ \phi \end{pmatrix} = R(\alpha) \begin{pmatrix} H_S \\ h \end{pmatrix}, \quad \text{with } R(\theta) = \begin{pmatrix} c_\theta & -s_\theta \\ s_\theta & c_\theta \end{pmatrix}. \quad (4)$$

The squared matrix elements M_{ij}^2 ($i, j = 1, 2$) in the basis (s, ϕ) are given in terms of the parameters in the potential as

$$M_{11}^2 = 2m_S^2 + v^2 \lambda_{\Phi S}, \quad M_{22}^2 = 2\lambda v^2, \quad M_{12}^2 = v\mu_{\Phi S}. \quad (5)$$

The mass eigenvalues for H_S (m_{H_S}) and h (m_h), and the mixing angle α are easily obtained:

$$m_{H_S}^2 = M_{11}^2 c_\alpha^2 + M_{22}^2 s_\alpha^2 + M_{12}^2 s_{2\alpha}, \quad m_h^2 = M_{11}^2 s_\alpha^2 + M_{22}^2 c_\alpha^2 - M_{12}^2 s_{2\alpha}, \quad t_{2\alpha} = \frac{2M_{12}^2}{M_{11}^2 - M_{22}^2}. \quad (6)$$

These relations can be inverted to express each element of the squared mass matrix in terms of the mass eigenvalues:

$$M_{11}^2 = m_{H_S}^2 c_\alpha^2 + m_h^2 s_\alpha^2, \quad M_{22}^2 = m_{H_S}^2 s_\alpha^2 + m_h^2 c_\alpha^2, \quad M_{12}^2 = \frac{1}{2} s_{2\alpha} (m_{H_S}^2 - m_h^2). \quad (7)$$

From Eqs. (5) and (6), we see that the decoupling limit is defined by $m_S^2 \rightarrow \infty$, where m_{H_S} and α become infinity and zero, respectively. On the other hand, the alignment limit is obtained by taking $\mu_{\Phi_S} \rightarrow 0$, in which the mixing angle α vanishes. In this limit, m_{H_S} is not necessarily large. Conversely, from the second equations of (5) and (7) we find that a large value of m_{H_S} with non-zero α is realized only by taking a large value of the quartic coupling λ . Therefore, in the case $\alpha \neq 0$, there must be an upper limit on m_{H_S} by imposing perturbative unitarity, vacuum stability and triviality bounds (see App. A). We will quantitatively derive such limit in the next section. Following the above discussion, the HSM can be described by 5 independent parameters after fixing the VEV v and m_h :

$$m_{H_S}, \quad s_\alpha, \quad \lambda_S, \quad \lambda_{\Phi_S}, \quad \mu_S. \quad (8)$$

The kinetic and Yukawa terms (here and in the following we explicitly write only those for the third generation fermions) are given by

$$\mathcal{L} = (D_\mu \Phi)^\dagger (D^\mu \Phi) + \frac{1}{2}(\partial_\mu S)(\partial^\mu S) - (y_t \bar{Q}_L^3 \Phi^c t_R + y_b \bar{Q}_L^3 \Phi b_R + y_\tau \bar{L}_L^3 \Phi \tau_R + \text{h.c.}), \quad (9)$$

where $Q_L^3 = (t, b)_L$ and $L_L^3 = (\nu_\tau, \tau)_L$ and $\Phi^c = i\tau_2 \Phi^*$. The covariant derivative for Φ reads

$$D_\mu \Phi = \partial_\mu \Phi - ig_2 \frac{\tau^a}{2} W_\mu^a \Phi - \frac{i}{2} g_1 B_\mu \Phi, \quad (10)$$

where g_2 and g_1 are the $SU(2)_L$ and $U(1)_Y$ gauge couplings, respectively. We see that the singlet field S does not couple to the SM fermions and gauge bosons, so that interaction terms for H_S with SM fields are only generated by the mixing. In terms of the mass eigenstates of the Higgs bosons, we thus obtain:

$$\mathcal{L}_{\text{int}} = \left(\frac{h}{v} c_\alpha + \frac{H_S}{v} s_\alpha \right) (2m_W^2 W_\mu^+ W^{-\mu} + m_Z^2 Z_\mu Z^\mu - m_f \bar{f} f), \quad (f = t, b, \tau). \quad (11)$$

B. 2-Higgs Doublet Model

In order to avoid tree level flavour changing neutral currents in the 2HDM, we impose a discrete Z_2 symmetry [17], which can be softly broken. The Z_2 charge assignment for the two doublets is: $(\Phi_1, \Phi_2) \rightarrow (+\Phi_1, -\Phi_2)$. The Higgs potential is given by

$$\begin{aligned} V(\Phi_1, \Phi_2)_{\text{2HDM}} = & \mu_1^2 |\Phi_1|^2 + \mu_2^2 |\Phi_2|^2 - \mu_{12}^2 (\Phi_1^\dagger \Phi_2 + \text{h.c.}) + \frac{1}{2} \lambda_1 |\Phi_1|^4 + \frac{1}{2} \lambda_2 |\Phi_2|^4 \\ & + \lambda_3 |\Phi_1|^2 |\Phi_2|^2 + \lambda_4 |\Phi_1^\dagger \Phi_2|^2 + \frac{1}{2} \lambda_5 [(\Phi_1^\dagger \Phi_2)^2 + \text{h.c.}], \end{aligned} \quad (12)$$

where μ_{12}^2 is the soft-breaking term of the Z_2 symmetry. In general, the μ_{12}^2 and λ_5 parameters can be complex, but we assume them to be real for simplicity.

A convenient basis for the Higgs fields is the so-called Higgs basis (Φ, Ψ) [18] which is related to the original one (Φ_1, Φ_2) by

$$\begin{pmatrix} \Phi_1 \\ \Phi_2 \end{pmatrix} = R(\beta) \begin{pmatrix} \Phi \\ \Psi \end{pmatrix}, \quad (13)$$

where $t_\beta = v_2/v_1$ with v_i the VEV of Φ_i . In this basis, the VEV $v(= \sqrt{v_1^2 + v_2^2})$ and the NG bosons (G^\pm and G^0) belong to the same doublet. Namely,

$$\Phi = \begin{pmatrix} G^+ \\ \frac{h'_1 + v + iG^0}{\sqrt{2}} \end{pmatrix}, \quad \Psi = \begin{pmatrix} H^+ \\ \frac{h'_2 + iA}{\sqrt{2}} \end{pmatrix}. \quad (14)$$

In Eq. (14), H^\pm and A are the physical singly-charged and CP-odd Higgs bosons, respectively. The two CP-even Higgs states h'_1 and h'_2 can mix each other. Their mass eigenstates are defined by

$$\begin{pmatrix} h'_1 \\ h'_2 \end{pmatrix} = R(\alpha - \beta) \begin{pmatrix} H \\ h \end{pmatrix}. \quad (15)$$

By imposing the tadpole conditions

$$\left. \frac{\partial V}{\partial h_1} \right|_0 = \left. \frac{\partial V}{\partial h_2} \right|_0 = 0, \quad (16)$$

we can eliminate μ_1^2 and μ_2^2 . The masses for A (m_A) and H^\pm (m_{H^\pm}) are then given by

$$m_{H^\pm}^2 = M^2 - \frac{v^2}{2}(\lambda_4 + \lambda_5), \quad m_A^2 = M^2 - v^2\lambda_5, \quad (17)$$

where $M^2 = \mu_{12}^2/(s_\beta c_\beta)$. The relation between the CP-even Higgs boson masses and the matrix elements M_{ij}^2 in the (h'_1, h'_2) basis is given in Eqs. (6) and (7) after the replacement of $(\alpha, H_S) \rightarrow (\alpha - \beta, H)$. The squared matrix elements are given in terms of the potential parameters by the following relations:

$$\begin{aligned} M_{11}^2 &= v^2(\lambda_1 c_\beta^4 + \lambda_2 s_\beta^4) + \frac{v^2}{2}\lambda_{345}s_{2\beta}^2, & M_{22}^2 &= M^2 + v^2 s_\beta^2 c_\beta^2 (\lambda_1 + \lambda_2 - 2\lambda_{345}), \\ M_{12}^2 &= v^2 s_\beta c_\beta (\lambda_2 s_\beta^2 - \lambda_1 c_\beta^2 + c_{2\beta} \lambda_{345}), \end{aligned} \quad (18)$$

where $\lambda_{345} = \lambda_3 + \lambda_4 + \lambda_5$. From the discussion above, the scalar potential can be fully described by the following set of independent parameters (after fixing v and m_h):

$$m_A, \quad m_{H^\pm}, \quad m_H, \quad c_{\beta-\alpha}, \quad t_\beta, \quad M^2, \quad (19)$$

with $0 < \beta - \alpha < \pi$.

Let us discuss the decoupling and the alignment limits in the 2HDM. The decoupling limit is given by $M^2 \rightarrow \infty$, by which all the masses of H^\pm , A and H become infinity, and $t_{2(\beta-\alpha)}$ becomes zero (equivalently $s_{\beta-\alpha} \rightarrow 1$). On the other hand, the alignment limit is defined by taking $s_{\beta-\alpha} \rightarrow 1$, so that the h'_1 state in Eq. (14) corresponds to the h state. Similarly to the HSM, if we take $s_{\beta-\alpha} \neq 1$ the decoupling limit cannot be reached, because a large value for m_H is only realized by a large value of the scalar quartic couplings (which are disfavored, e.g., by perturbative unitarity). This is clear from the relation:

$$M_{11}^2 = m_H^2 c_{\beta-\alpha}^2 + m_h^2 s_{\beta-\alpha}^2 = v^2 \left(\lambda_1 c_\beta^4 + \lambda_2 s_\beta^4 + \frac{\lambda_{345}}{2} s_{2\beta}^2 \right). \quad (20)$$

Regarding the kinetic and Yukawa interaction terms, they are given by

$$\mathcal{L} = \sum_{i=1,2} (D_\mu \Phi_i)^\dagger (D^\mu \Phi_i) - (y_t \bar{Q}_L^3 \Phi_t^c t_R + y_b \bar{Q}_L^3 \Phi_b b_R + y_\tau \bar{L}_L^3 \Phi_\tau \tau_R + \text{h.c.}), \quad (21)$$

where the covariant derivative D_μ is the same as Eq. (10). The Φ_f ($f = t, b, \tau$) fields are Φ_1 or Φ_2 depending on the Z_2 -charge assignment for the right handed fermions. For the latter, there are 4 independent choices which lead to 4 different types of Yukawa interactions [19, 20], referred to as Type-I, Type-II, Type-X and Type-Y [21]. The combination of $(\Phi_t, \Phi_b, \Phi_\tau)$ is determined in each type as follows:

$$\begin{aligned} (\Phi_t, \Phi_b, \Phi_\tau) &= (\Phi_2, \Phi_2, \Phi_2) \quad \text{for Type-I,} \\ (\Phi_t, \Phi_b, \Phi_\tau) &= (\Phi_2, \Phi_1, \Phi_1) \quad \text{for Type-II,} \\ (\Phi_t, \Phi_b, \Phi_\tau) &= (\Phi_2, \Phi_2, \Phi_1) \quad \text{for Type-X,} \\ (\Phi_t, \Phi_b, \Phi_\tau) &= (\Phi_2, \Phi_1, \Phi_2) \quad \text{for Type-Y.} \end{aligned} \quad (22)$$

For example, Type-II is realized by setting the charge assignments as $(t_R, b_R, \tau_R) \rightarrow (-t_R, +b_R, +\tau_R)$ and taking all the left-handed fermions to be Z_2 -even. In terms of the

Higgs boson mass eigenstates, we obtain the following interaction terms:

$$\begin{aligned}
\mathcal{L}_{\text{int}} &= \left(\frac{h}{v} s_{\beta-\alpha} + \frac{H}{v} c_{\beta-\alpha} \right) (2m_W^2 W_\mu^+ W^{-\mu} + m_Z^2 Z_\mu Z^\mu) \\
&\quad - \sum_{f=t,b,\tau} \frac{m_f}{v} [(s_{\beta-\alpha} + \xi_f c_{\beta-\alpha}) \bar{f} f h + (c_{\beta-\alpha} - \xi_f s_{\beta-\alpha}) \bar{f} f H - 2i I_f \xi_f \bar{f} \gamma_5 f A] \\
&\quad - \frac{\sqrt{2}}{v} [\bar{t}(m_b \xi_b P_R - m_t \xi_t P_L) b H^+ + \bar{\nu}_\tau m_\tau \xi_\tau P_R \tau H^+ + \text{h.c.}], \tag{23}
\end{aligned}$$

where $I_f = +1/2(-1/2)$ for $f = t(b, \tau)$ and $P_{L,R}$ are the projection operators for left-/right-handed fermions. The mixing factors ξ_f are given by:

$$\begin{aligned}
\xi_t &= \cot \beta \text{ for all Types} \\
\xi_b &= \cot \beta \text{ for Type-I, -X, } -\tan \beta \text{ for Type-II, -Y} \\
\xi_\tau &= \cot \beta \text{ for Type-I, -Y, } -\tan \beta \text{ for Type-II, -X.}
\end{aligned} \tag{24}$$

It is straightforward to check that, in the alignment limit $s_{\beta-\alpha} \rightarrow 1$, all the h couplings coincide with those of the SM Higgs boson at tree level.

C. Georgi-Machacek Model

The Higgs potential in the GM model can be constructed in terms of the $SU(2)_L \times SU(2)_R$ bi-doublet Φ and bi-triplet Δ fields:

$$\Phi \equiv (\Phi^c, \Phi) = \begin{pmatrix} \phi^{0*} & \phi^+ \\ -\phi^- & \phi^0 \end{pmatrix}, \quad \Delta \equiv (\chi^c, \xi, \chi) = \begin{pmatrix} \chi^{0*} & \xi^+ & \chi^{++} \\ -\chi^- & \xi^0 & \chi^+ \\ \chi^{--} & -\xi^- & \chi^0 \end{pmatrix}, \tag{25}$$

where $\chi^c = C_3 \chi^*$ is the charge conjugated χ field with

$$C_3 = \begin{pmatrix} 0 & 0 & 1 \\ 0 & -1 & 0 \\ 1 & 0 & 0 \end{pmatrix}. \tag{26}$$

The neutral component fields are expressed by

$$\phi^0 = \frac{1}{\sqrt{2}}(\phi_r + v_\phi + i\phi_i), \quad \chi^0 = \frac{1}{\sqrt{2}}(\chi_r + i\chi_i) + v_\chi, \quad \xi^0 = \xi_r + v_\xi, \tag{27}$$

where v_ϕ , v_χ and v_ξ being the VEV's for ϕ^0 , χ^0 and ξ^0 , respectively.

Assuming the vacuum alignment: $v_\chi = v_\xi (\equiv v_\Delta)$, the VEV $\langle \Delta \rangle$ is proportional to the 3×3 identity matrix. In this configuration, the global $SU(2)_L \times SU(2)_R$ symmetry is spontaneously broken down to the $SU(2)_V$ symmetry, i.e., the so-called custodial symmetry.

The most general scalar potential for the Φ and Δ fields is given by

$$\begin{aligned} V(\Phi, \Delta)_{\text{GM}} &= \mu_\Phi^2 \text{tr}(\Phi^\dagger \Phi) + \mu_\Delta^2 \text{tr}(\Delta^\dagger \Delta) + \lambda_1 [\text{tr}(\Phi^\dagger \Phi)]^2 + \lambda_2 [\text{tr}(\Delta^\dagger \Delta)]^2 + \lambda_3 \text{tr}[(\Delta^\dagger \Delta)^2] \\ &+ \lambda_4 \text{tr}(\Phi^\dagger \Phi) \text{tr}(\Delta^\dagger \Delta) + \lambda_5 \text{tr} \left(\Phi^\dagger \frac{\tau^a}{2} \Phi \frac{\tau^b}{2} \right) \text{tr}(\Delta^\dagger t^a \Delta t^b) \\ &+ \mu_1 \text{tr} \left(\Phi^\dagger \frac{\tau^a}{2} \Phi \frac{\tau^b}{2} \right) (P^\dagger \Delta P)^{ab} + \mu_2 \text{tr} (\Delta^\dagger t^a \Delta t^b) (P^\dagger \Delta P)^{ab}, \end{aligned} \quad (28)$$

where τ^a and t^a ($a = 1-3$) are the 2×2 and 3×3 matrix representations of the $SU(2)$ generators, respectively. The unitary matrix P enters in the similarity transformation $P(-i\epsilon^a)P^\dagger = t^a$ with ϵ^a being the adjoint representation of the $SU(2)$ generators. The explicit form of P is given as

$$P = \begin{pmatrix} -1/\sqrt{2} & i/\sqrt{2} & 0 \\ 0 & 0 & 1 \\ 1/\sqrt{2} & i/\sqrt{2} & 0 \end{pmatrix}. \quad (29)$$

We note that the custodial symmetry in the Higgs potential is broken by the $U(1)_Y$ hypercharge gauge interaction at one-loop level. The effects of the loop induced custodial-breaking terms, which cannot be described in terms of Φ and Δ , were discussed in Ref. [22].

The mass eigenstates of the physical Higgs bosons can be classified in terms of the $SU(2)_V$ multiplets, namely, the 5-plet $(H_5^{\pm\pm}, H_5^\pm, H_5^0)$, the two 3-plets (H_3^\pm, H_3^0) and (G^\pm, G^0) , and the two singlets H_1 and h . The Higgs bosons belonging to the same $SU(2)_V$ multiplet are degenerate in mass. These mass eigenstates are related to the original states given in Eq. (25) by the following transformations:

$$\begin{aligned} \begin{pmatrix} \chi_i \\ \phi_i \end{pmatrix} &= R(\beta) \begin{pmatrix} G^0 \\ H_3^0 \end{pmatrix}, \\ \begin{pmatrix} \phi^\pm \\ \xi^\pm \\ \chi^\pm \end{pmatrix} &= R_5^\pm \begin{pmatrix} \phi^\pm \\ \xi'^\pm \\ H_5^\pm \end{pmatrix} = R_5^\pm R_\beta \begin{pmatrix} G^\pm \\ H_3^\pm \\ H_5^\pm \end{pmatrix}, \quad \begin{pmatrix} \xi_r \\ \phi_r \\ \chi_r \end{pmatrix} = R_5^r \begin{pmatrix} \xi'_r \\ \phi_r \\ H_5^0 \end{pmatrix} = R_5^r R_\alpha \begin{pmatrix} H_1 \\ h \\ H_5^0 \end{pmatrix}, \end{aligned} \quad (30)$$

where R_5^\pm and R_5^r are the orthogonal 3×3 matrices which separate the 5-plet Higgs bosons from the other singly-charged and CP-even scalar states, respectively. Their explicit forms

are given by

$$R_5^\pm = \begin{pmatrix} 1 & 0 & 0 \\ 0 & \frac{1}{\sqrt{2}} & -\frac{1}{\sqrt{2}} \\ 0 & \frac{1}{\sqrt{2}} & \frac{1}{\sqrt{2}} \end{pmatrix}, \quad R_5^r = \begin{pmatrix} \frac{1}{\sqrt{3}} & 0 & -\sqrt{\frac{2}{3}} \\ 0 & 1 & 0 \\ \sqrt{\frac{2}{3}} & 0 & \frac{1}{\sqrt{3}} \end{pmatrix}. \quad (31)$$

The other two matrices involved in Eq. (30) are

$$R_\beta = \begin{pmatrix} s_\beta & c_\beta & 0 \\ c_\beta & -s_\beta & 0 \\ 0 & 0 & 1 \end{pmatrix}, \quad R_\alpha = \begin{pmatrix} c_\alpha & -s_\alpha & 0 \\ s_\alpha & c_\alpha & 0 \\ 0 & 0 & 1 \end{pmatrix}, \quad (32)$$

where $t_\beta = v_\phi/(2\sqrt{2}v_\Delta)$ and α describes the mixing of the CP-even singlet states. By using the two independent tadpole conditions

$$\left. \frac{\partial V}{\partial \phi_r} \right|_0 = \left. \frac{\partial V}{\partial \chi_r} \right|_0 = 0, \quad (33)$$

we can eliminate the μ_Φ^2 and μ_Δ^2 parameters. The mass eigenvalues of the $SU(2)_V$ 5-plet and 3-plet Higgs bosons (m_{H_5} and m_{H_3}) are then given by

$$m_{H_5}^2 = v^2 \left(\lambda_3 c_\beta^2 - \frac{3}{2} \lambda_5 s_\beta^2 \right) - \frac{v\mu_1}{\sqrt{2}} t_\beta s_\beta - 3\sqrt{2}v\mu_2 c_\beta, \quad m_{H_3}^2 = -\frac{v^2}{2} \lambda_5 - \frac{v\mu_1}{\sqrt{2}c_\beta}. \quad (34)$$

The relation between the masses of the CP-even Higgs bosons and the matrix elements M_{ij}^2 in the basis of (ξ'_r, ϕ_r) can be obtained by using Eqs. (6) and (7) after the replacement of $H_S \rightarrow H_1$. The matrix elements have the following expressions in terms of the potential parameters:

$$\begin{aligned} M_{11}^2 &= v^2(3\lambda_2 + \lambda_3)c_\beta^2 - \frac{v\mu_1}{\sqrt{2}}t_\beta s_\beta + \frac{3v\mu_2}{\sqrt{2}}c_\beta, \\ M_{22}^2 &= 8v^2\lambda_1 s_\beta^2, \\ M_{12}^2 &= \sqrt{\frac{3}{2}} \left[v^2(2\lambda_4 + \lambda_5)c_\beta + \frac{v\mu_1}{\sqrt{2}} \right] s_\beta. \end{aligned} \quad (35)$$

Summarizing, the GM model can be described by 7 independent quantities, after fixing v and m_h :

$$m_{H_5}, \quad m_{H_3}, \quad m_{H_1}, \quad t_\beta, \quad s_\alpha, \quad \mu_1, \quad \mu_2. \quad (36)$$

Let us now discuss the decoupling and the alignment limits. The decoupling limit is realized by taking $t_\beta \rightarrow \infty$ with a negative value of μ_1 . In this limit, m_{H_3} and m_{H_5} become

infinity as seen by Eq. (34). In addition, among the matrix elements given in Eq. (35), only M_{11}^2 becomes infinity, so that we obtain $m_{H_1} \rightarrow \infty$ and $\alpha \rightarrow 0$. Differently from the HSM and the 2HDM, the alignment limit cannot be taken without the decoupling limit, because $t_\beta \rightarrow \infty$ is necessarily required in order to have the doublet field Φ carrying the whole VEV v .

Finally, let us explicitly write the kinetic and Yukawa Lagrangian terms of the GM model:

$$\mathcal{L} = \frac{1}{2}\text{tr}(D_\mu \Phi)^\dagger (D^\mu \Phi) + \frac{1}{2}\text{tr}(D_\mu \Delta)^\dagger (D^\mu \Delta) - (y_t \bar{Q}_L^3 \Phi^c t_R + y_b \bar{Q}_L^3 \Phi b_R + y_\tau \bar{L}_L^3 \Phi \tau_R + \text{h.c.}), \quad (37)$$

where the covariant derivatives are expressed as

$$D_\mu \Phi = \partial_\mu \Phi - ig_2 \frac{\tau^a}{2} W_\mu^a \Phi + ig_1 B_\mu \Phi \frac{\tau^3}{2}, \quad (38)$$

$$D_\mu \Delta = \partial_\mu \Delta - ig_2 t^a W_\mu^a \Delta + ig_1 B_\mu \Delta t^3. \quad (39)$$

The trilinear interaction terms of the physical Higgs bosons with SM fermions and gauge bosons are given by:

$$\begin{aligned} \mathcal{L}_{\text{int}} = & \frac{2m_W^2}{v} \left(c_{hVV} h + c_{H_1VV} H_1 - \frac{c_\beta}{\sqrt{3}} H_5^0 \right) W_\mu^+ W^{-\mu} \\ & + \frac{m_Z^2}{v} \left(c_{hVV} h + c_{H_1VV} H_1 + \frac{2c_\beta}{\sqrt{3}} H_5^0 \right) Z_\mu Z^\mu \\ & - \sum_{f=t,b,\tau} \frac{m_f}{v} \left(\frac{c_\alpha}{s_\beta} \bar{f} f h + \frac{s_\alpha}{s_\beta} \bar{f} f H_1 - 2i I_f \cot \beta \bar{f} \gamma_5 f H_3^0 \right) \\ & - \frac{\sqrt{2}}{v} \cot \beta \left[\bar{t} (m_b P_R - m_t P_L) b H_3^+ + \bar{\nu}_\tau m_\tau P_R \tau H_3^+ + \text{h.c.} \right], \end{aligned} \quad (40)$$

where

$$c_{hVV} = s_\beta c_\alpha - \frac{2\sqrt{6}}{3} c_\beta s_\alpha, \quad c_{H_1VV} = s_\beta s_\alpha + \frac{2\sqrt{6}}{3} c_\beta c_\alpha. \quad (41)$$

There are several remarkable points to be stressed about the interaction terms given in Eq. (40). First, the 5-plet Higgs bosons have a fermiophobic nature, i.e., they do not couple to fermions, but they couple to the SM gauge bosons. Second, the coupling structure of the 3-plet Higgs bosons H_3^0 and H_3^\pm is the same as that for A and H^\pm in the Type-I 2HDM. Finally, the SM-like Higgs boson h coupling to the gauge bosons can be larger than the SM prediction, because of the factor of $2\sqrt{6}/3$ as shown in Eq. (41). This is a peculiarity of the GM model, because $\kappa_V \leq 1$ in the HSM and the 2HDMs.

In Table II, we summarize the relevant properties of the three extended Higgs sectors here considered.

	Decoupling limit	Alignment limit	$\kappa_V \equiv g_{hVV}/g_{hVV}^{\text{SM}}$	$\kappa_f \equiv g_{hff}/g_{hff}^{\text{SM}}$
HSM	$m_S^2 \rightarrow \infty$	$s_\alpha \rightarrow 0$	c_α	c_α
2HDM	$M^2 \rightarrow \infty$	$s_{\beta-\alpha} \rightarrow 1$	$s_{\beta-\alpha}$	$s_{\beta-\alpha} + \xi_f c_{\beta-\alpha}$
GM model	$t_\beta \rightarrow \infty$	$t_\beta \rightarrow \infty$	$s_\beta c_\alpha - 2\sqrt{2/3} c_\beta s_\alpha$	c_α/s_β

TABLE II: Summary of the relevant properties of the HSM, the 2HDM and the GM model.

III. UPPER BOUND ON THE EXTRA HIGGS BOSON MASSES

As discussed in the previous section, if the alignment limit is not realized, there must be an upper bound on the extra Higgs boson masses. In this section, we numerically evaluate such upper bound by taking into account perturbative unitarity, vacuum stability and triviality constraints. In addition, we will concern about the compatibility with the experimental values of the S and T parameters introduced by Peskin and Takeuchi [23] which describe the oblique corrections to the electroweak processes. In particular, we require the predictions of $\Delta S \equiv S_{\text{NP}} - S_{\text{SM}}$ and $\Delta T \equiv T_{\text{NP}} - T_{\text{SM}}$ to be within the 95% CL region of the $\Delta\chi^2$ fit (corresponding to $\Delta\chi^2 \leq 5.99$), where S_{NP} (T_{NP}) and S_{SM} (T_{SM}) are the New Physics and the SM prediction for the S (T) parameters, respectively. The observed values of ΔS and ΔT are [24]

$$\Delta S_{\text{exp}} = 0.05 \pm 0.09, \quad \Delta T_{\text{exp}} = 0.08 \pm 0.07, \quad (42)$$

with the correlation factor ρ_{ST} being 0.91. The analytic formulae for ΔS and ΔT are given in Appendix C for each of the extended Higgs models.

We introduce $M_{2\text{nd}}$ as the mass of the next-to-lightest Higgs boson, assuming the lightest one to be the discovered Higgs boson h . By definition, $M_{2\text{nd}}$ corresponds to m_{H_S} in the HSM, while in the 2HDM and the GM model, it is defined by:

$$\begin{aligned} M_{2\text{nd}} &= \text{Min}(m_{H^\pm}, m_A, m_H) \quad \text{in the 2HDM,} \\ M_{2\text{nd}} &= \text{Min}(m_{H_5}, m_{H_3}, m_{H_1}) \quad \text{in the GM model.} \end{aligned} \quad (43)$$

In the following analysis, we enforce the bounds in two steps denoted by ‘‘Bound A’’ and ‘‘Bound B’’. First, we impose the tree level perturbative unitarity, the vacuum stability and the constraint from the S and T parameters (Bound A). In addition to the constraints of Bound A, we then impose the improved vacuum stability and the triviality constraints

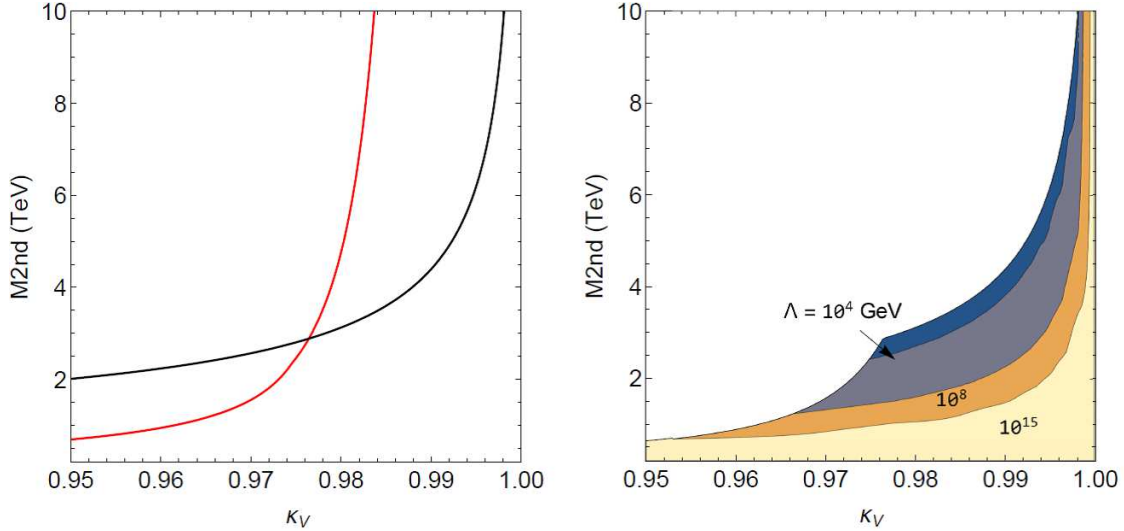


FIG. 1: Bounds on $M_{2\text{nd}} = m_{H_S}$ in the HSM as functions of $\kappa_V = g_{hVV}/g_{hVV}^{\text{SM}}$. On the left panel, we show the upper limit on $M_{2\text{nd}}$ given by the tree level perturbative unitarity and the vacuum stability constraints (black line) and that given by the electroweak S and T parameters (red line). On the right panel, the upper limit on $M_{2\text{nd}}$ is shown by imposing Bound B, where the cutoff of the theory is shown as contours on this plane.

(Bound B) evaluated by using the running coupling constants arising from the one-loop renormalization group equations (RGEs) (see Appendix B). Thus, Bound A does not depend on the energy scale, while Bound B does. In particular, Bound B depends on the theory cutoff connected with the appearance of Landau poles or vacuum instability, both requiring further contributions from a more fundamental theory. Let us discuss the results for the HSM. We scan over the parameters λ_{Φ_S} , λ_S and μ_S of the potential and, in the left panel of Fig. 1, we show the upper bound on $M_{2\text{nd}} = m_{H_S}$ as a function of $\kappa_V = g_{hVV}/g_{hVV}^{\text{SM}}$ under Bound A. We separately take into account the perturbative unitarity and vacuum stability constraints (black curve) and the constraints from the S and T parameters (red curve). We can see that, at $\kappa_V \simeq 0.975$, the constraint providing the most stringent bound on $M_{2\text{nd}}$ is interchanged, namely, for $\kappa_V \lesssim 0.975$ it is the one from the S and T parameters, while for $\kappa_V \gtrsim 0.975$, the perturbative unitarity and the vacuum stability bounds give the stronger bound. When κ_V is getting close to 1, the bound on $M_{2\text{nd}}$ becomes milder and it disappears in the alignment limit $\kappa_V \rightarrow 1$.

On the right panel, we show the allowed values of $M_{2\text{nd}}$ under Bound B as a function of

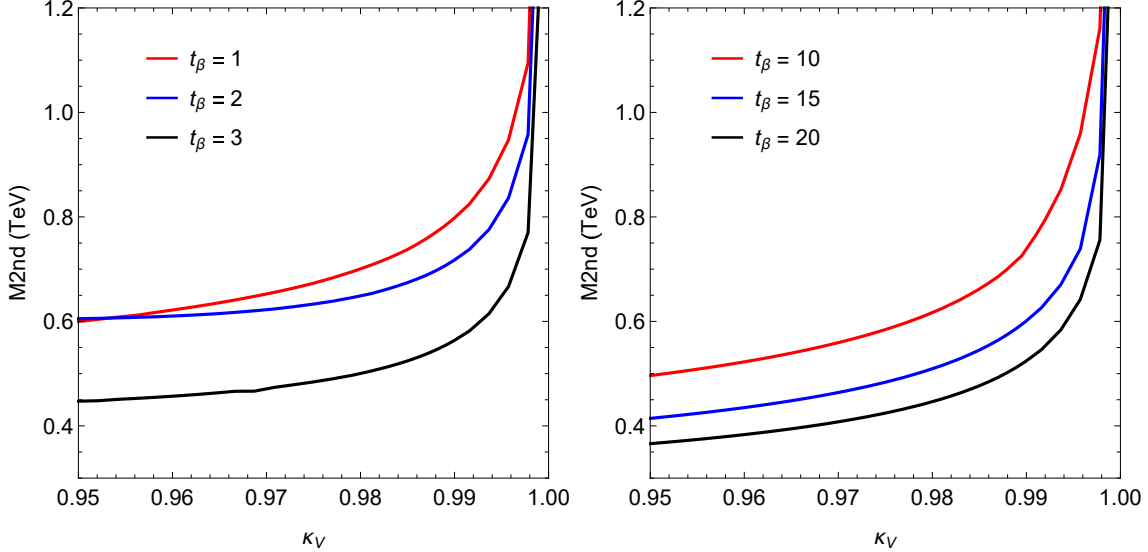


FIG. 2: Upper limit on $M_{2\text{nd}} = \text{Min}(m_{H^\pm}, m_A, m_H)$ obtained by imposing Bound A as a function of κ_V in the 2HDMs with $t_\beta = 1, 2, 3$ (left panel) and $t_\beta = 10, 15, 20$ (right panel).

κ_V . The cutoff scale Λ of the theory is indicated by the contours in this plot. We conclude that, if the deviation in the hVV coupling from the SM prediction is measured to be, e.g., larger than 1% ($\kappa_V \leq 0.99$), the extra Higgs boson mass in the HSM is expected to be below ~ 4 TeV. Furthermore, if we require the theory cutoff to be larger than e.g., 10^8 (10^{15}) GeV, then the extra Higgs boson mass is expected to be below ~ 2 (1) TeV, assuming $\kappa_V \leq 0.99$. In other words, if there is no other NP contribution modifying the running of the coupling constants of the HSM up to 10^{15} GeV, then a 1% deviation in the hVV coupling implies a bound on the extra Higgs boson mass around 1 TeV. As shown in Sec. IV, these values are still allowed by direct searches and by the signal strength analysis at the LHC.

Next, we derive the upper limit on $M_{2\text{nd}}$ in the 2HDM. The values of m_H , m_A , m_{H^\pm} and M^2 are scanned so as to extract the maximal value of $M_{2\text{nd}}$ for each fixed value of t_β and κ_V . We also scan over the sign of $c_{\beta-\alpha}$. In Fig. 2, we show the upper limit on $M_{2\text{nd}}$ as a function of κ_V obtained by imposing Bound A. The left (right) panel shows the result for the case with $\tan\beta = 1, 2$ and 3 ($10, 15$ and 20). Regardless the value of t_β , the maximally allowed value of $M_{2\text{nd}}$ is getting small as $|\kappa_V - 1|$ becomes large. For example, for $\kappa_V \leq 0.99$, we find the upper limit on $M_{2\text{nd}}$ to be about 800, 550 and 500 GeV for $\tan\beta = 1, 3$ and 20 , respectively. Similar to the HSM, the bound disappears in the alignment limit $\kappa_V \rightarrow 1$.

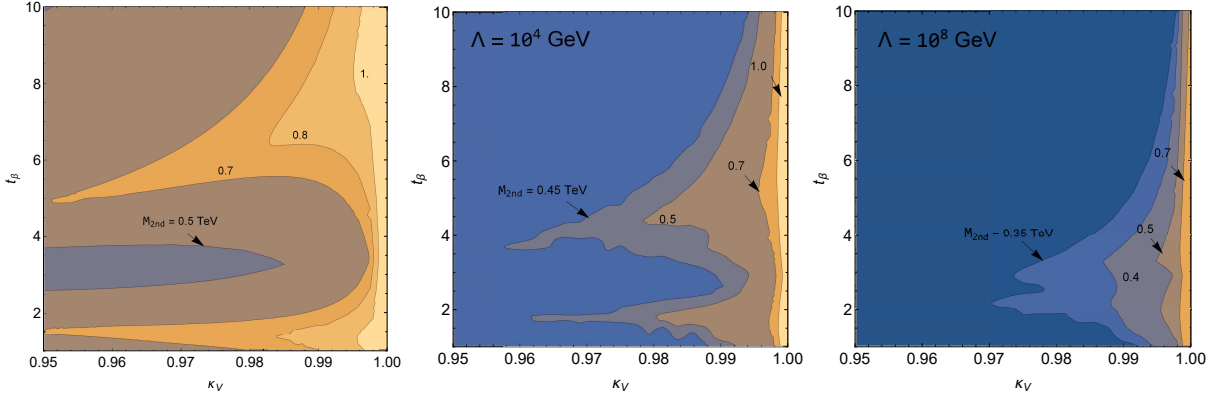


FIG. 3: Contour plots for the maximally allowed value of $M_{2\text{nd}} = \text{Min}(m_{H^\pm}, m_A, m_H)$ in the 2HDMs obtained by imposing Bound A (left), Bound B with $\Lambda = 10^4$ GeV (center) and Bound B with $\Lambda = 10^8$ GeV (right) on the κ_V - t_β plane.

We can see that the extracted limit on $M_{2\text{nd}}$ in the 2HDM (typically less than 1 TeV) is much smaller than that given in the HSM (typically a few TeV). We note that this result does not depend on the type of Yukawa interaction. In Fig. 3, we show the contour plot for the maximally allowed value of $M_{2\text{nd}}$ in the 2HDM on the κ_V - t_β plane. The left panel is obtained by imposing Bound A, while the center and right panels correspond to Bound B with $\Lambda = 10^4$ GeV (center) and 10^8 GeV (right). Let us first discuss the left panel. For a fixed value of κ_V , the maximally allowed value of $M_{2\text{nd}}$ strongly depends on t_β (according to Fig. 2) and $M_{2\text{nd}}$ is typically expected to be below 1 TeV, also for κ_V quite close to 1. If we impose Bound B (center and right panels), the allowed values of $M_{2\text{nd}}$ become significantly smaller than those in the left panel. As an example, for $\Lambda = 10^8$ GeV, $M_{2\text{nd}} \lesssim 400$ GeV is expected if $\kappa_V \leq 0.99$. We note that the dependence on the type of the Yukawa interactions only appears through the bottom Yukawa terms in the β functions (see Appendix B), so it is negligibly small and Fig. 3 bounds are applicable to all the 2HDM Types. As shown in Sec. IV for the 2HDM, the LHC bounds obtained after the first run 2 data analysis are already competitive with the theoretical ones here derived.

Finally, let us discuss the results in the GM model. The values of m_{H_5} , m_{H_3} , m_{H_1} , μ_1 and μ_2 are scanned with an enough wide range to extract the maximal value of $M_{2\text{nd}}$ for each fixed value of t_β and κ_V . For a fixed value of t_β , there can be two possible values of α giving the same value of κ_V (e.g., for $t_\beta = 3$, both $\alpha \simeq -0.91$ and $\alpha \simeq -0.087$ give $\kappa_V = 0.99$),

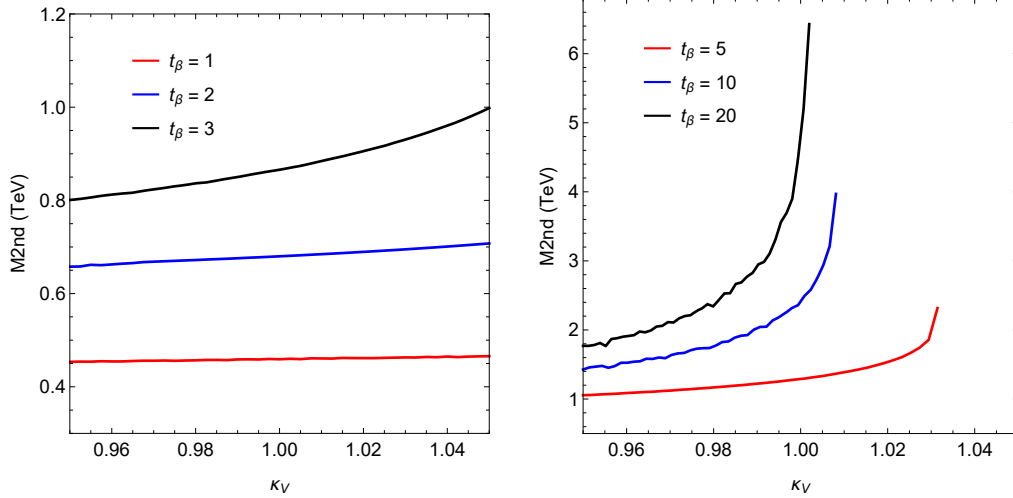


FIG. 4: Upper limit on $M_{2\text{nd}} = \text{Min}(m_{H_5}, m_{H_3}, m_{H_1})$ obtained by imposing Bound A as a function of κ_V in the GM model with $t_\beta = 1, 2, 3$ (left panel) and $t_\beta = 5, 10, 20$ (right panel).

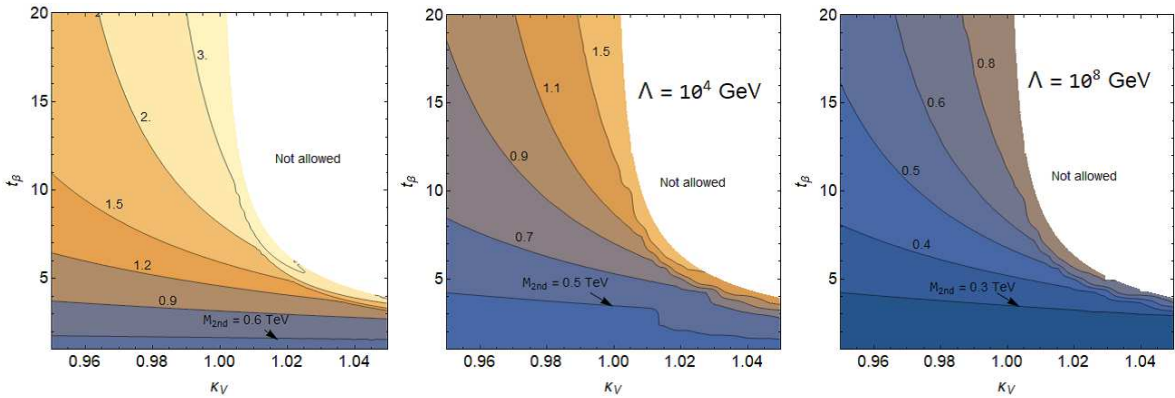


FIG. 5: Contour plots for the maximally allowed value of $M_{2\text{nd}} = \text{Min}(m_{H_5}, m_{H_3}, m_{H_1})$ in the GM model obtained by imposing Bound A (left), Bound B with $\Lambda = 10^4$ GeV (center) and Bound B with $\Lambda = 10^8$ GeV (right) on the κ_V - t_β plane.

so we here consider both values of α . In Fig. 4, we show the maximally allowed value of $M_{2\text{nd}}$ as a function of κ_V by imposing Bound A for $t_\beta = 1, 2$ and 3 (left panel) and 5, 10 and 20 (right panel). As we mentioned in Sec. IIC, $\kappa_V > 1$ is allowed and its maximal value is found at $t_\alpha = -2\sqrt{6}/(3t_\beta)$. For example, for $t_\beta = 3(5)$, we obtain $\text{Max}(\kappa_V) \simeq 1.08(1.03)$. For this reason, there is an end point in the curves shown on the right panel. We find that the maximal allowed value of $M_{2\text{nd}}$ monotonically increases as κ_V is getting large. However, as long as we take a finite value of t_β , there is always an upper limit on $M_{2\text{nd}}$, i.e., the

decoupling limit cannot be taken unless $t_\beta \rightarrow \infty$ (corresponding to the alignment limit).

In Fig. 5, we show the contour plots for $M_{2\text{nd}}$ on the κ_V - t_β plane by imposing Bound A (left) and by imposing Bound B with $\Lambda = 10^4$ GeV (center) and 10^8 GeV (right). The white regions are not allowed due to the existence of a maximal value for κ_V . We can see that the maximal value of $M_{2\text{nd}}$ is smoothly getting large when t_β and/or κ_V becomes large. As compared to the case of the 2HDMs, $M_{2\text{nd}}$ can be typically above 1 TeV when we take a large value of t_β . For example, for $\kappa_V < 0.99$, we obtain the maximal allowed value of $M_{2\text{nd}}$ to be about 1 (2) TeV in the case of $t_\beta = 5(10)$. If we impose Bound B, the maximal $M_{2\text{nd}}$ becomes smaller, but still $M_{2\text{nd}} > 1$ TeV is allowed for $\kappa_V < 0.99$ with $\Lambda = 10^4$ GeV.

IV. COMPLEMENTARITY BETWEEN EXPERIMENTAL AND THEORETICAL BOUNDS

In this section, we discuss the complementarity between the bounds discussed in Sec. III and those from the LHC data. For the former, we impose Bound A which does not depend on the cutoff Λ . For the latter, we take into account the bounds from direct searches for additional Higgs bosons and from the data for the discovered Higgs boson $h(125)$. As we saw in the previous section, Bound A provides an upper limit on $M_{2\text{nd}}$ depending on the value of κ_V . Conversely, bounds from LHC data typically provide a lower limit on the mass of the extra Higgs boson. Therefore, by combining these two types of bounds, we can further narrow down the possible allowed region for $M_{2\text{nd}}$ for each extended Higgs model.

Here, we consider the masses of extra Higgs bosons to be above 350 GeV, i.e., beyond the threshold of the decay of neutral Higgs bosons into $t\bar{t}$. For the 2HDM and the GM model, we take $t_\beta \geq 1$, because the case with $t_\beta < 1$ is highly disfavored by the various B physics experiments [25, 26].

Let us discuss the bounds from direct searches. In the aforementioned scenarios, the main decay modes of the extra Higgs bosons are the following:

$$H_S \rightarrow t\bar{t}/VV/hh \quad (\text{in the HSM}), \quad (44)$$

$$H \rightarrow t\bar{t}/VV/hh, \quad A \rightarrow t\bar{t}/Zh, \quad H^\pm \rightarrow tb/W^\pm h \quad (\text{in the 2HDM}), \quad (45)$$

$$H_1 \rightarrow t\bar{t}/VV/hh, \quad H_3^0 \rightarrow t\bar{t}/Zh, \quad H_3^\pm \rightarrow tb/W^\pm h, \\ H_5^0 \rightarrow VV, \quad H_5^\pm \rightarrow W^\pm Z, \quad H_5^{\pm\pm} \rightarrow W^\pm W^\pm \quad (\text{in the GM model}), \quad (46)$$

where $V = W, Z$. We note that in the 2HDM with $s_{\beta-\alpha} = 1$, the main decay mode of the extra neutral Higgs bosons becomes $H/A \rightarrow t\bar{t}$, but it can be replaced by the other 2-fermion final states in the Type-II, -X, -Y 2HDMs if we take a large enough value of t_β . For example, for $\tan\beta \gtrsim 6(10)$, $s_{\beta-\alpha} = 1$, and $m_\Phi (= m_H = m_A = m_{H^\pm}) = M = 500$ GeV, the channel $H/A \rightarrow b\bar{b}$ ($H/A \rightarrow \tau\tau$) can be dominant instead of the $t\bar{t}$ mode in the Type-II (-X) 2HDM². However, as we will show below, in a large t_β scenario i.e., $t_\beta = \mathcal{O}(10)$, the production cross section of the extra Higgs bosons is highly suppressed, so that the constraint on the mass of the extra Higgs boson becomes weak regardless of the type of Yukawa interaction³.

First, let us discuss the searches for additional neutral Higgs bosons (\mathcal{H}). We here consider the following processes:

$$(i) \quad gg \rightarrow \mathcal{H} \rightarrow t\bar{t}, \quad (ii) \quad gg \rightarrow \mathcal{H} \rightarrow hh, \quad (iii) \quad gg \rightarrow \mathcal{H} \rightarrow ZZ, \quad (iv) \quad gg \rightarrow \mathcal{H} \rightarrow Zh. \quad (47)$$

We note that, although there are other production modes for \mathcal{H} such as the vector boson fusion and the vector boson associated processes, the cross section of these modes are negligibly small in the scenario with $\kappa_V \sim 1$. Thus, we only take into account the gluon fusion production in this analysis. Regarding the top quark associated production, the search for $pp \rightarrow t\bar{t}\mathcal{H}$ followed by $\mathcal{H} \rightarrow t\bar{t}$ decay has been performed at the LHC using the data of 13 TeV and 13.2 fb^{-1} [29]. The current bound assuming 100% of the $\text{BR}(\mathcal{H} \rightarrow t\bar{t})$ is, however, not so stringent. For example in the 2HDMs (regardless the type of Yukawa interactions), no bound on the mass of H has been taken when $\tan\beta \gtrsim 0.3$. Therefore, the top quark associated process will be neglected in this analysis⁴. The processes (i)–(iv) have been searched for using the 8 TeV data with the integrated luminosity of 20.3 fb^{-1} in Refs. [30], [31], [32] and [33], respectively. Due to the fact that there is no significant excess in the number of signal events with respect to that given in the SM, the 95% CL upper limit on the cross section times the branching ratio has been provided for each process. Concerning the process (ii),

² In the Type-X 2HDM, $H^\pm \rightarrow tb$ can also be replaced by $H^\pm \rightarrow \tau^\pm\nu$ for $t_\beta \gtrsim 10$, $s_{\beta-\alpha} = 1$, and $m_\Phi = M = 500$ GeV. This is not the case for the other 2HDM types.

³ In the LHC Run-2 and the High-Luminosity LHC experiments, the large t_β scenario can also be constrained [27, 28] via the pair production of the extra Higgs bosons, whose cross section does not depend on t_β .

⁴ In the HSM, the production cross section of $pp \rightarrow t\bar{t}H_S$ is proportional to s_α^2 , so that the search for $H_S \rightarrow t\bar{t}$ is less important with respect to the 2HDM as long as we take $s_\alpha \ll 1$. In the GM model, the properties of H_1 and H_3^0 are quite similar to those of H and A in the Type-I 2HDM, respectively, so that we can apply the similar phenomenological analysis of the Type-I 2HDM for these neutral Higgs bosons.

the $hh \rightarrow \gamma\gamma b\bar{b}$, $\tau\tau b\bar{b}$, $WW^*b\bar{b}$ and $b\bar{b}b\bar{b}$ decay modes were independently analysed [31], and similarly for the process (iv), for which the $h \rightarrow b\bar{b}$ and $h \rightarrow \tau\tau$ modes were analysed [33].

In order to compare the bounds driven by the experiments with the corresponding theory predictions, let us evaluate the cross section for the gluon fusion production for \mathcal{H} ($\sigma_{gg\mathcal{H}}$) by using the following approximation:

$$\sigma_{gg\mathcal{H}} \simeq \sigma_{ggh_{\text{SM}}} \times \frac{\Gamma(\mathcal{H} \rightarrow gg)}{\Gamma(h_{\text{SM}} \rightarrow gg)}, \quad (48)$$

where $\sigma_{ggh_{\text{SM}}}$ is the gluon fusion cross section in the SM and $\Gamma(X \rightarrow gg)$ is the decay rate for the $X \rightarrow gg$ mode. The reference values of $\sigma_{ggh_{\text{SM}}}$ at 8 TeV are given in [34].

Second, let us discuss direct searches for singly-charged Higgs bosons. Typical main decay modes are given in Eqs. (45) and (46) in the 2HDM and the GM model, respectively. The search for charged Higgs bosons decaying into the $t\bar{b}$ mode has been surveyed in Ref. [29]. The current bound is not so stringent. For example, in the Type-II 2HDM no bound has been taken on the mass of H^\pm when $t_\beta \gtrsim 0.5$, which is also valid for all the other types of Yukawa interaction. For the Wh decay mode, there is no available current limit. Detailed simulation studies for the H^\pm search including the Wh mode at the LHC Run-2 has been done in Ref. [35] for the Type-II 2HDM. Concerning the WZ channel, which is relevant for H_5^\pm in the GM model only, it has been searched via the WZ boson fusion process in Ref. [36] using the 13 TeV data with the integrated luminosity of 15.2 fb^{-1} . This gives the lower limit on t_β (corresponding to the upper limit on v_Δ) for a fixed value of m_{H_5} . For example, for $m_{H_5} = 500 \text{ GeV}$, $t_\beta \lesssim 1.65$ ($v_\Delta \gtrsim 45 \text{ GeV}$) is excluded at 95% CL. Actually, this limit is much weaker than the one given by the search for $H_5^{\pm\pm} \rightarrow W^\pm W^\pm$, so that imposing the latter bound discussed below will be enough.

Third, the search for doubly-charged Higgs bosons in the same-sign diboson decay channel has been performed at the LHC using the 8 TeV data sample with the integrated luminosity of 19.4 fb^{-1} in Ref. [37]. The 95% CL upper limit on the cross section of the $W^\pm W^\pm$ fusion process times the branching ratio of the $H_5^{\pm\pm} \rightarrow W^\pm W^\pm$ mode has been provided. From this result, we can extract the 95% CL lower (upper) limit on the value of t_β (v_Δ) for a fixed value of m_{H_5} . Since the $H_5^{\pm\pm} W^\mp W^\mp$ coupling is proportional to v_Δ , the vector boson fusion cross section of $H_5^{\pm\pm}$ ($\sigma_{H_5^{\pm\pm}}$) for an arbitrary value of v_Δ can be extracted as follows:

$$\sigma_{H_5^{\pm\pm}} = \left(\frac{v_\Delta}{v_{\Delta}^{\text{Ref.}}} \right)^2 \times \sigma_{H_5^{\pm\pm}} \Big|_{v_{\Delta}^{\text{Ref.}}}, \quad (49)$$

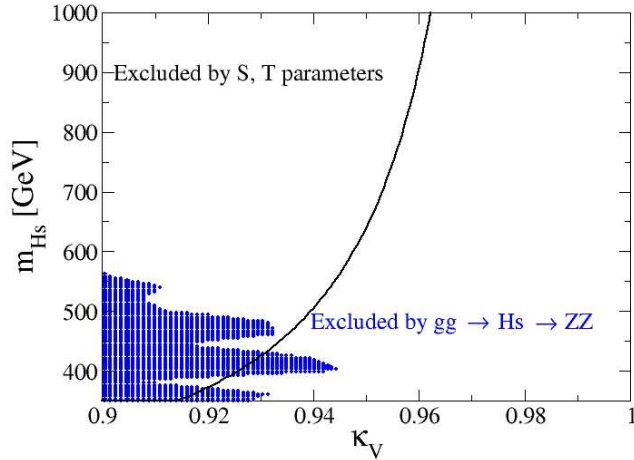


FIG. 6: Allowed parameter space on the κ_V - m_{H_S} plane in the HSM. The blue shaded region is excluded by the search for the $gg \rightarrow H_S \rightarrow ZZ$ process. The region above the black solid curve is excluded by the S and T parameters. In this plot, we take $\lambda_{\Phi S} = \mu_S = \lambda_S = 0$.

where $v_{\Delta}^{\text{Ref.}}$ is a reference value of v_{Δ} which is set to be 16, 25 and 35 GeV in Ref. [37]. The values of $\sigma_{H_5^{\pm\pm}}|_{v_{\Delta}^{\text{Ref.}}}$ are also presented in Ref. [37].

Apart from the direct searches for extra Higgs bosons, we need to consider also the constraint on the parameter space from the $h(125)$ data at the LHC. Here, we take into account the signal strengths μ_X for $X = \gamma\gamma, ZZ, WW$ and $\tau\tau$ defined by

$$\mu_X \equiv \sigma_{ggh} \times \text{BR}(h \rightarrow XX). \quad (50)$$

The measured values of μ_X are given by the combined analysis of the ATLAS and CMS experiments using the LHC Run-1 data [1] as follows:

$$\mu_{\gamma\gamma} = 1.10_{-0.22}^{+0.23}, \quad \mu_{ZZ} = 1.13_{-0.31}^{+0.34}, \quad \mu_{WW} = 0.84_{-0.17}^{+0.17}, \quad \mu_{\tau\tau} = 1.0_{-0.6}^{+0.6}, \quad (51)$$

and we shall require each prediction for μ_X to lie within the 95% CL region.

In Fig. 6, we show the allowed parameter space on the κ_V - m_{H_S} plane in the HSM. The region above the black solid curve is excluded at 95% CL by the S and T parameters, while the blue shaded region is excluded at 95% CL by the direct search for the $gg \rightarrow H_S \rightarrow ZZ$ process, which turns out to set the most stringent constraint among the direct search and signal strength data. However, we see that the region excluded by the direct searches is

almost ruled out by the constraint from the S, T parameters, so that the LHC data do not significantly improve our bounds for m_{H_S} with respect to Sec. III.

Next, the constraints on the parameter space of the 2HDM are shown in Figs. 7 and 8. In Fig. 7, we show the excluded region at 95% CL by the direct searches (shaded region) and μ_X (indicated by the green dashed line) on the $c_{\beta-\alpha}-m_\Phi$ plane, where $m_\Phi = m_A = m_{H^\pm} = m_H$. We also display the corresponding value of κ_V on the top horizontal axis. The results in the Type-I, -II, -X and -Y 2HDMs are shown from the top to bottom panels, while those for $t_\beta = 1, 2$ and 3 are shown from the left to right panels. In all the plots, we take $M = m_\Phi$. Regardless of the type of Yukawa interactions, the bound from the direct searches becomes milder when we take a larger value of t_β , because the top quark loop contribution to the gluon fusion cross section is suppressed by a factor $\propto \cot^2 \beta$. In fact, if we take $t_\beta \gtrsim 10$, almost no region on the $c_{\beta-\alpha}-m_\Phi$ plane shown in this figure is excluded by the direct searches. Concerning the bound from μ_X , they give a severe constraint on κ_V particularly in the Type-II and Type-Y 2HDMs, by which $|\kappa_V - 1|$ larger than 1% are not allowed. This constraint tends to get stronger when we take a larger value of t_β except for the Type-I 2HDM. Let us now comment on the case with $M \neq m_\Phi$. For $m_\Phi < M$, the constraint from $gg \rightarrow H \rightarrow hh$ tends to be milder, because the branching ratio of $H \rightarrow hh$ becomes small. On the contrary, the constraint from $gg \rightarrow H \rightarrow ZZ$ tends to be slightly stronger due to a little enhancement of the branching ratio of $H \rightarrow ZZ$. In any case, the total excluded region with $M < m_\Phi$ is found not to change so much with respect to our initial assumption. On the contrary, the case $M > m_\Phi$ is totally disfavored by the vacuum stability bound.

Let us combine the bounds from the LHC data discussed above and Bound A in the 2HDM. In Fig. 8, the black (red) dots are allowed by only Bound A (both Bound A and the LHC data). We here keep the assumption of the degeneracy in mass of the extra Higgs bosons, and we scan over the value of M . The results for Type-I and Type-II 2HDMs are shown on the left and right panels, respectively, and the value of t_β is taken to be 1, 2, 3 and 10 from the top to bottom panels. We note that the results for the Type-X and Type-Y 2HDMs are almost the same as those for the Type-I and Type-II 2HDMs, respectively. We can see that for $t_\beta = 1$ (top panels), $m_\Phi \lesssim 600$ GeV is excluded, because of the $gg \rightarrow H/A \rightarrow t\bar{t}$ process (according to Fig. 7). For larger t_β , the region filled by the black and red dots is getting the same in the Type-I 2HDM, namely, the bounds from the direct search and μ_X become less important. In contrast, in the Type-II 2HDM, the region

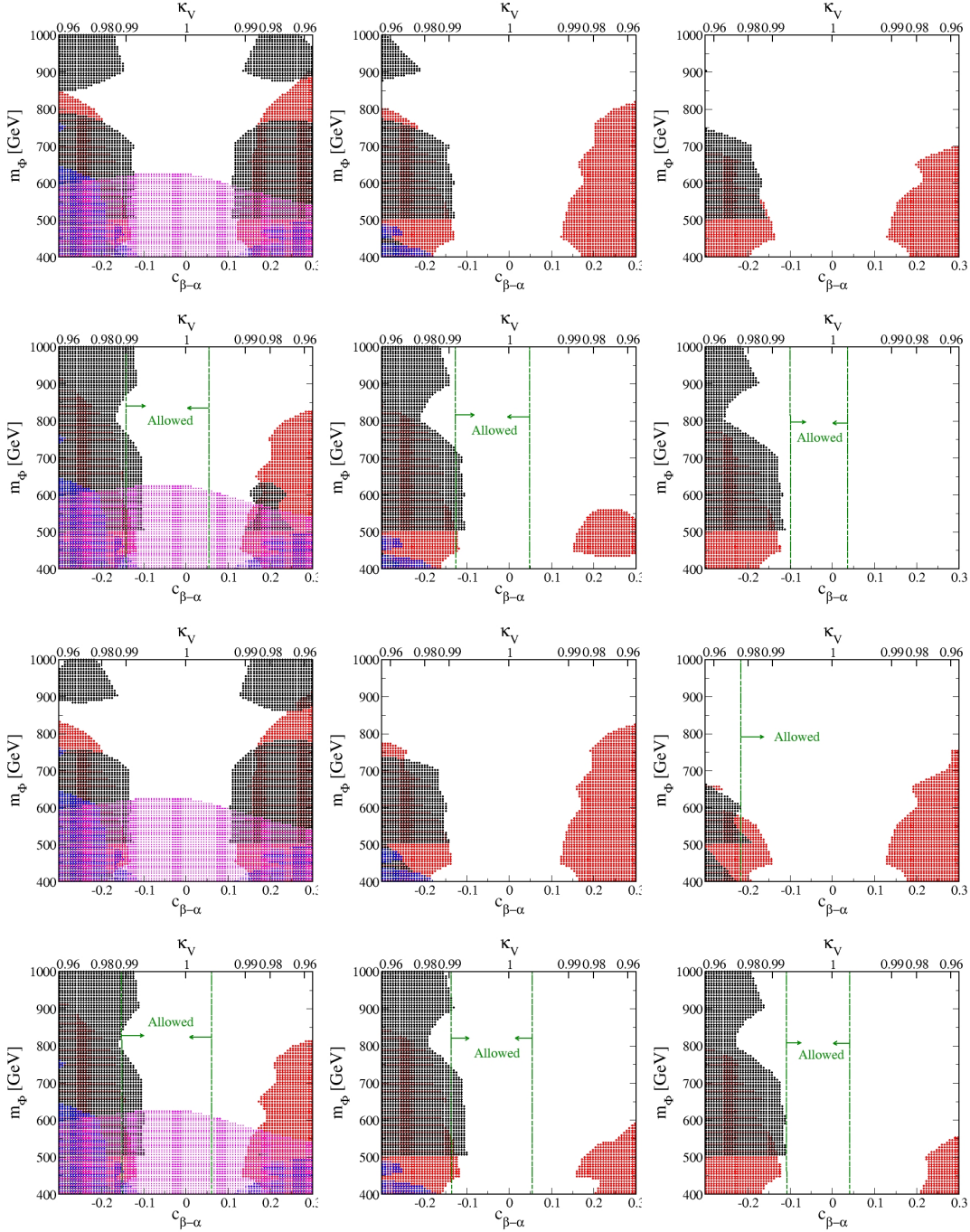


FIG. 7: Constraints on the parameter space with $M/m_\Phi = 1$ in the 2HDMs, where $\tan\beta$ is taken to be 1 (left), 2 (center) and 3 (right). The top to bottom panels show the results in the Type-I, -II, -X and -Y 2HDMs. The shaded regions are excluded by the direct searches at the LHC: $gg \rightarrow H \rightarrow hh$ (black), $gg \rightarrow A \rightarrow Zh$ (red), $gg \rightarrow H \rightarrow ZZ$ (blue), and $gg \rightarrow H/A \rightarrow t\bar{t}$ (magenta). The region outside the green dashed curves is excluded by the 95% CL Higgs signal strength constraints.

filled by the red dots is much smaller than that filled by the black dots even for the case

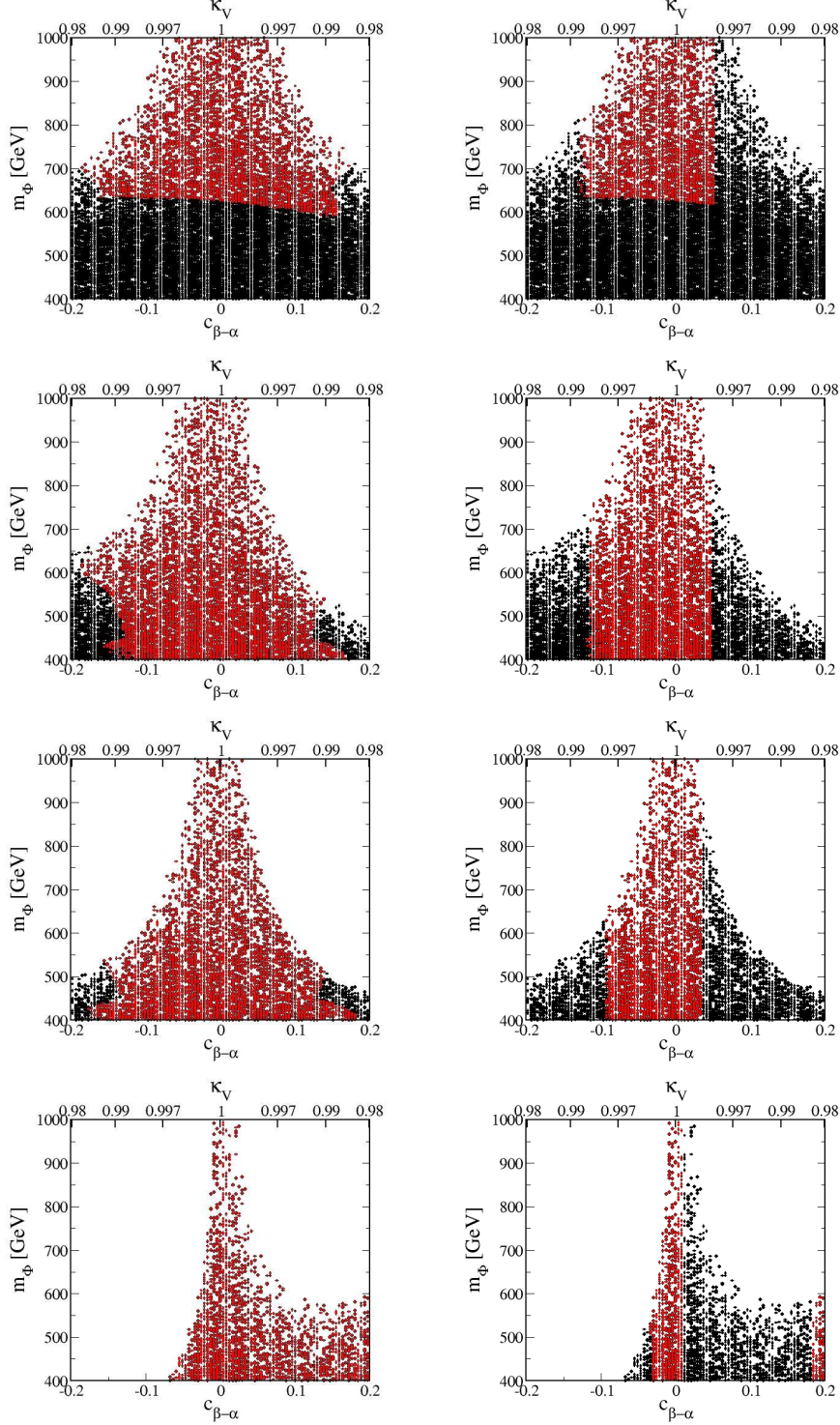


FIG. 8: Black (Red) dots are allowed only by Bound A (by both Bound A and the LHC data) in the Type-I (left) and Type-II (right) 2HDMs. The value of $\tan\beta$ is taken to be 1, 2, 3 and 10 from the top to bottom panels. The value of M is scanned to be from 0 to $m_\Phi (= m_{H^\pm} = m_A = m_H)$.

with large t_β , because of the constraint from μ_X . In conclusion, we find that for smaller

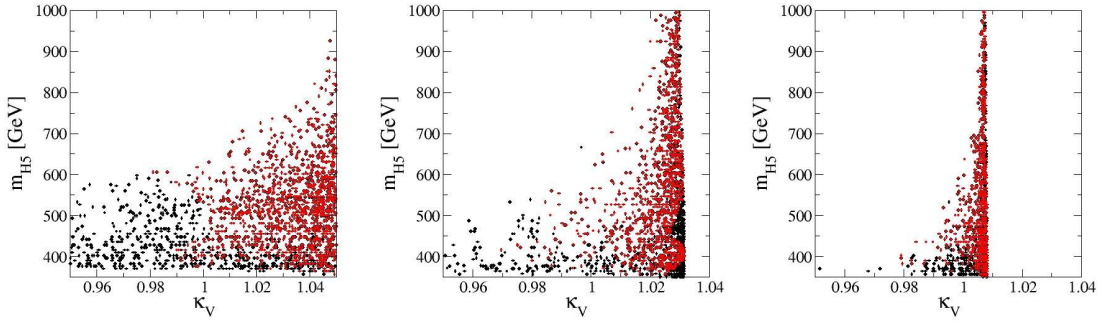


FIG. 9: Black (Red) dots are allowed only by Bound A (by both Bound A and the LHC data) in the GM model. The value of $\tan\beta$ is taken to be 3, 5 and 10 on the left, center and right panels, respectively. We take $m_{H_3} = m_{H_5}$. All the other parameters (m_{H_1} , μ_1 and μ_2) are scanned keeping $m_{H_1} \geq 350$ GeV.

values of t_β , $\kappa_V \lesssim 0.98(0.99)$ is excluded in the Type-I and X (Type-II and Y) 2HDMs. For larger values of t_β , a smaller value of κ_V , e.g., less than 0.98, is possible in all the four types, but the mass of the extra Higgs bosons has to be below ~ 600 GeV due to the theoretical constraints.

Finally, let us discuss the results in the GM model with $m_{H_5} = m_{H_3}$. In Fig. 9, similar to Fig 8, the black (red) dots are allowed by Bound A (by both Bound A and the LHC data). The parameters m_{H_1} , μ_1 and μ_2 are scanned ($m_{H_1} \geq 350$ GeV) with a large enough range to maximize the allowed parameter space. We note that the case with $t_\beta \lesssim 3$ is excluded by the direct searches for $H_5^{\pm\pm} \rightarrow W^\pm W^\pm$ up to m_{H_5} to be 800 GeV [37]. We see that a larger value of m_{H_5} is allowed in the case with $\kappa_V > 1$ by both the constraints from Bound A and the LHC data. For larger t_β , the allowed range of κ_V is getting smaller. For example, we obtain $0.96 \lesssim \kappa_V \lesssim 1.03$ and $0.99 \lesssim \kappa_V \lesssim 1.01$ for $t_\beta = 5$ and 10, respectively, if we require $m_{H_5} \geq 500$ GeV. Differently from the cases of the HSM and the 2HDM, even when $\kappa_V \simeq 1$ is considered, there is an upper limit on the mass of the extra Higgs bosons, because $\kappa_V \rightarrow 1$ does not correspond to the alignment limit in the GM model with any finite value of t_β .

In summary, the constraints on the extra Higgs boson masses from the currently available LHC data, including both the direct searches for extra Higgs bosons and the $h(125)$ signal strengths, strongly depend on the model considered. In particular, no further excluded regions were found by imposing the LHC data in the HSM for $\kappa_V \gtrsim 0.95$. In the 2HDMs,

it is necessary to distinguish among the different types of Yukawa interactions and the values of t_β . Assuming mass degeneracy for the extra Higgs bosons, in Type-I and -X 2HDMs for, e.g., $\kappa_V = 0.99$ the combined LHC data and theoretical constraints require $600 \text{ GeV} \lesssim M_{2\text{nd}} \lesssim 800 \text{ GeV}$ for $t_\beta = 1$, while, for $t_\beta = 10$, only the theoretical ones are relevant and one finds $M_{2\text{nd}} \lesssim 600 \text{ GeV}$. Conversely, the Type-II and -Y 2HDMs turn out to be more constrained by the LHC data with respect to the Type-I and -X 2HDMs because of the $h(125)$ signal strength bounds, the large t_β region being especially disfavored (in fact, almost only the alignment limit is allowed). Regarding the GM model, the LHC data definitely favor the region with $\kappa_V \gtrsim 1$, which shrinks closer to $\kappa_V = 1$ for larger values of t_β . For each value of κ_V which fulfills the LHC data constraints, the bounds on the extra Higgs boson masses are driven by the theoretical issues: e.g., for $\kappa_V = 1.01$ and $t_\beta = 5$, one finds $m_{H_{3,5}} \lesssim 700 \text{ GeV}$ (assuming $m_{H_3} = m_{H_5}$).

V. CONCLUSIONS

We have extracted the mass scale of a possible second Higgs boson $M_{2\text{nd}}$ by imposing theoretical constraints and by requiring compatibility with the currently available experimental data in the next-to-minimal Higgs models with $\rho = 1$ at tree level, namely the HSM, the 2HDMs and the GM model. In particular, we have focused on the correlation between the bound on $M_{2\text{nd}}$ and a possible deviation in the hVV ($V = W, Z$) couplings from the SM prediction. In doing so, we have assumed the discovered Higgs boson $h(125)$ to be the lightest state among all the other Higgs bosons. As for the theoretical bounds, we took into account perturbative unitarity, vacuum stability and triviality, while, as for the experimental constraints, we imposed the bounds from the electroweak precision data, the direct searches for extra Higgs bosons and the $h(125)$ signal strengths μ_X . Assuming a value of $\Delta\kappa_V \equiv \kappa_V - 1$, the non-LHC bounds (theoretical and EWPT constraints) enforce an upper limit on $M_{2\text{nd}}$, while the LHC data provide a lower bound. For the former, we applied Bound A and Bound B under the full scan of the model parameters. Our results are summarized in Table III for reference values of $\Delta\kappa_V$, assuming the cutoff to be above 10 TeV under Bound B. In addition, we have discussed the complementarity between the non-LHC and the LHC bounds, i.e., the direct searches and the $h(125)$ signal strengths. In the HSM, the LHC data do not improve the non-LHC bounds for $\kappa_V \gtrsim 0.95$. On the

$\Delta\kappa_V$	HSM	2HDM			GM Model		
		$t_\beta = 1$	$t_\beta = 2$	$t_\beta = 10$	$t_\beta = 3$	$t_\beta = 5$	$t_\beta = 10$
-1%	4.0 (3.5)	0.8 (0.5)	0.7 (0.5)	0.7 (0.4)	0.9 (0.4)	1.2 (0.6)	2.0 (1.0)
-2%	3.0 (2.5)	0.7 (0.4)	0.7 (0.5)	0.6 (0.3)	0.8 (0.4)	1.1 (0.6)	1.8 (0.9)
-5%	0.7 (0.7)	0.6 (0.3)	0.6 (0.4)	0.5 (0.3)	0.8 (0.4)	1.0 (0.6)	1.5 (0.8)
+1%	-	-	-	-	0.9 (0.5)	1.4 (0.7)	4.8 (1.8)

TABLE III: Summary of the upper bounds on $M_{2\text{nd}}$ (TeV) by Bound A (by Bound B requiring the cutoff scale to be above 10 TeV) in the models considered for reference values of $\Delta\kappa_V$.

contrary, in the 2HDMs, the constraint from the LHC data can be important depending on the type of Yukawa interaction and the value of t_β . For the Type-I and Type-X 2HDMs with $t_\beta \sim 1$, the LHC data restrict $\kappa_V \gtrsim 0.98$ and the mass of extra Higgs bosons to be above ~ 600 GeV. For larger t_β , the LHC data are less effective and they provide no further constraint with respect to the non-LHC bounds. For the Type-II and Type-Y 2HDMs, the μ_X data constrain $\kappa_V \gtrsim 0.99$ for $t_\beta \sim 1$, and such bound becomes stronger for larger t_β . Finally, in the GM model, we found that the case with $\kappa_V \gtrsim 1$ is favored by both the LHC and non-LHC bounds. In addition, for a larger value of t_β , the allowed range of κ_V is getting smaller. For example, if we require $m_{H_5}(=m_{H_3}) \geq 500$ GeV, we obtain $0.96 \lesssim \kappa_V \lesssim 1.03$ and $0.99 \lesssim \kappa_V \lesssim 1.01$ for $t_\beta = 5$ and 10, respectively.

In conclusion, from the analysis performed in this paper, we have clarified the connection between the scale of the second Higgs boson mass in the non-minimal Higgs sectors here considered and the deviation in the hVV couplings from the SM prediction. Since the hVV couplings will be precisely measured at future collider experiments such as the High-Luminosity LHC (a few percent level) and e^+e^- colliders (less than 1% level at the International Linear Collider [38] with 500 GeV of the collision energy [9]), we can obtain precise information of the mass of the next-to-lightest Higgs boson even without its discovery at the LHC.

Appendix A: Theoretical constraints

We briefly review the theoretical constraints, i.e., the perturbative unitarity, the vacuum stability and the triviality we enforce in the models with an extended Higgs sector. We then present relevant analytic expressions for these constraints.

We first discuss the bound from the perturbative unitarity. The request of the S-matrix unitarity for 2 body to 2 body elastic scattering processes for scalar bosons, assuming the validity of perturbative calculations, leads to the following condition:

$$|\text{Re}(a_J)| \leq 1/2, \quad (\text{A1})$$

where a_J are partial wave amplitudes with total angular momentum J . For the purpose of this paper, we define the perturbative unitarity bound by

$$|x_i| \leq 1/2, \quad (\text{A2})$$

where x_i are the eigenvalues of the S -wave ($J = 0$) amplitude matrix, because they give the most stringent constraints.

In the HSM, we obtain 4 independent eigenvalues [39, 40]

$$x_1^\pm = \frac{1}{16\pi} \left[3\lambda + 6\lambda_S \pm \sqrt{(6\lambda_S - 3\lambda)^2 + 4\lambda_{\Phi S}^2} \right], \quad (\text{A3})$$

$$x_2 = \frac{1}{8\pi} \lambda, \quad (\text{A4})$$

$$x_3 = \frac{1}{8\pi} \lambda_{\Phi S}. \quad (\text{A5})$$

In the 2HDMs, we obtain 12 independent eigenvalues [11–14]

$$x_1^\pm = \frac{1}{32\pi} \left[3(\lambda_1 + \lambda_2) \pm \sqrt{9(\lambda_1 - \lambda_2)^2 + 4(2\lambda_3 + \lambda_4)^2} \right], \quad (\text{A6})$$

$$x_2^\pm = \frac{1}{32\pi} \left[(\lambda_1 + \lambda_2) \pm \sqrt{(\lambda_1 - \lambda_2)^2 + 4\lambda_4^2} \right], \quad (\text{A7})$$

$$x_3^\pm = \frac{1}{32\pi} \left[(\lambda_1 + \lambda_2) \pm \sqrt{(\lambda_1 - \lambda_2)^2 + 4\lambda_5^2} \right], \quad (\text{A8})$$

$$x_4^\pm = \frac{1}{16\pi} (\lambda_3 + 2\lambda_4 \pm 3\lambda_5), \quad (\text{A9})$$

$$x_5^\pm = \frac{1}{16\pi} (\lambda_3 \pm \lambda_4), \quad (\text{A10})$$

$$x_6^\pm = \frac{1}{16\pi} (\lambda_3 \pm \lambda_5). \quad (\text{A11})$$

In the GM model, we obtain 9 independent eigenvalues [41, 42]

$$x_1^\pm = \frac{1}{16\pi} \left[12\lambda_1 + 22\lambda_2 + 14\lambda_3 \pm \sqrt{(12\lambda_1 - 22\lambda_2 - 14\lambda_3)^2 + 144\lambda_4^2} \right], \quad (\text{A12})$$

$$x_2^\pm = \frac{1}{16\pi} \left[4\lambda_1 + 4\lambda_2 - 2\lambda_3 \pm \sqrt{(4\lambda_1 - 4\lambda_2 + 2\lambda_3)^2 + 4\lambda_5^2} \right], \quad (\text{A13})$$

$$x_3 = \frac{1}{16\pi} (8\lambda_2 + 16\lambda_3), \quad (\text{A14})$$

$$x_4 = \frac{1}{16\pi} (8\lambda_2 + 4\lambda_3), \quad (\text{A15})$$

$$x_5 = \frac{1}{16\pi} 4(\lambda_4 + \lambda_5), \quad (\text{A16})$$

$$x_6 = \frac{1}{16\pi} (4\lambda_4 - 2\lambda_5), \quad (\text{A17})$$

$$x_7 = \frac{1}{16\pi} 4(\lambda_4 + \lambda_5). \quad (\text{A18})$$

As stated above, we impose $|x_i| \leq 1/2$ and derive the allowed regions in the parameter space of each model.

Next, let us discuss the vacuum stability bound. We require that the scalar potential is bounded from below in any direction with large field values. This can be simply expressed by $V^{(4)} \geq 0$, where $V^{(4)}$ is the scalar quartic part of the potential. The sufficient and necessary conditions to satisfy the vacuum stability constraint in the HSM [5, 43] are given by

$$\lambda \geq 0, \quad \lambda_S \geq 0, \quad 2\sqrt{\lambda\lambda_S} + \lambda_{\Phi_S} \geq 0. \quad (\text{A19})$$

In the 2HDMs, the sufficient and necessary conditions are expressed by:

$$\lambda_1 \geq 0, \quad \lambda_2 \geq 0, \quad \sqrt{\lambda_1\lambda_2} + \lambda_3 + \text{MIN}(0, \lambda_4 + \lambda_5, \lambda_4 - \lambda_5) \geq 0. \quad (\text{A20})$$

Eqs. (A19) and (A20) can be improved by using the running couplings evaluated by solving the one-loop RGEs (see App. B) and requiring that all the above inequalities are satisfied at every energy scale μ with $m_Z \leq \mu \leq \Lambda$, where Λ is the cutoff of the theory.

In the GM model, it has been clarified in Ref. [22, 44] that the custodial symmetry in the potential is explicitly broken due to the $U(1)_Y$ gauge boson loop effects. In order to make the model consistent at high energies, we need to use the most general form of the Higgs potential without the custodial symmetry. The explicit form of the general potential is given in Eq. (D1) in App. D. In terms of the quartic couplings of the general potential, the necessary conditions to guarantee the vacuum stability are derived by assuming two non-vanishing complex fields at once. Taking into account all the possible two field directions, we obtain the following inequalities:

$$\begin{aligned}
\lambda &\geq 0, \quad \rho_3 \geq 0, \quad \rho_1 + \rho_2 \geq 0, \quad \rho_1 + \frac{\rho_2}{2} \geq 0, \\
\rho_4 + \frac{\rho_5}{2} + \sqrt{2\rho_3(\rho_1 + \rho_2)} &\geq 0, \\
\rho_4 + \sqrt{2\rho_3(\rho_1 + \rho_2)} &\geq 0, \\
\rho_4 + 2\sqrt{\rho_3(2\rho_1 + \rho_2)} &\geq 0, \\
\rho_4 + \rho_5 + 2\sqrt{\rho_3(2\rho_1 + \rho_2)} &\geq 0, \\
\sigma_1 + 2\sqrt{\lambda(\rho_1 + \rho_2)} &\geq 0, \\
\sigma_1 + \sigma_2 + 2\sqrt{\lambda(\rho_1 + \rho_2)} &\geq 0, \\
\sigma_1 + \frac{\sigma_2}{2} + \sqrt{2\lambda(2\rho_1 + \rho_2)} &\geq 0, \\
\sigma_3 + \sqrt{2\lambda\rho_3} &\geq 0.
\end{aligned} \tag{A21}$$

Appendix B: One-loop β -functions

We here present the set of β -functions evaluated at one-loop level in the HSM, the 2HDMs and the GM model. The β -function for a coupling constant y is defined by

$$\beta(y) \equiv \frac{d}{d \ln \mu} y. \tag{B1}$$

The RGE evolution of the gauge, scalar and Yukawa couplings is given by the following β -functions in the HSM [5]:

$$\beta(g_3) = \frac{g_3^3}{16\pi^2}(-7), \quad \beta(g_2) = \frac{g_2^3}{16\pi^2} \left(-\frac{19}{6} \right), \quad \beta(g_1) = \frac{g_1^3}{16\pi^2} \left(\frac{41}{6} \right), \tag{B2}$$

$$\beta(y_t) = \frac{1}{16\pi^2} \left[\frac{9}{2}y_t^3 + \frac{3}{2}y_b^3 - y_t \left(8g_3^2 + \frac{9}{4}g_2^2 + \frac{17}{12}g_1^2 \right) \right], \tag{B3}$$

$$\beta(y_b) = \frac{1}{16\pi^2} \left[\frac{9}{2}y_b^3 + \frac{3}{2}y_t^3 - y_b \left(8g_3^2 + \frac{9}{4}g_2^2 + \frac{5}{12}g_1^2 \right) \right], \tag{B4}$$

$$\begin{aligned}
\beta(\lambda) = \frac{1}{16\pi^2} \left\{ 24\lambda^2 + 2\lambda_{\Phi S}^2 - 6(y_t^4 + y_b^4) + \frac{9}{8}g_2^4 + \frac{3}{8}g_1^4 + \frac{3}{4}g_1^2g_2^2 \right. \\
\left. - 3\lambda[3g_2^2 + g_1^2 - 4(y_t^2 + y_b^2)] \right\},
\end{aligned} \tag{B5}$$

$$\beta(\lambda_{\Phi S}) = \frac{1}{16\pi^2} \left[12\lambda\lambda_{\Phi S} + 8\lambda_{\Phi S}^2 + 24\lambda_{\Phi S}\lambda_S - \lambda_{\Phi S} \left(\frac{9}{2}g_2^2 + \frac{3}{2}g_1^2 - 6y_t^2 - 6y_b^2 \right) \right], \tag{B6}$$

$$\beta(\lambda_S) = \frac{1}{16\pi^2} (2\lambda_{\Phi S}^2 + 72\lambda_S^2). \tag{B7}$$

In the 2HDMs, we obtain

$$\beta(g_3) = \frac{g_3^3}{16\pi^2}(-7), \quad \beta(g_2) = \frac{g_2^3}{16\pi^2}(-3), \quad \beta(g_1) = \frac{g_1^3}{16\pi^2}7, \quad (\text{B8})$$

$$\beta(y_t) = \frac{1}{16\pi^2} \left[\frac{9}{2}y_t^3 + \frac{3}{2}y_b^3\Theta - y_t \left(8g_3^2 + \frac{9}{4}g_2^2 + \frac{17}{12}g_1^2 \right) \right], \quad (\text{B9})$$

$$\beta(y_b) = \frac{1}{16\pi^2} \left[\frac{9}{2}y_b^3 + \frac{3}{2}y_t^3\Theta - y_b \left(8g_3^2 + \frac{9}{4}g_2^2 + \frac{5}{12}g_1^2 \right) \right], \quad (\text{B10})$$

$$\beta(\lambda_1) = \frac{1}{16\pi^2} \left[12\lambda_1^2 + 4\lambda_3^2 + 2\lambda_4^2 + 4\lambda_3\lambda_4 + 2\lambda_5^2 - 12y_b^4\tilde{\Theta} + \frac{9}{4}g_2^4 + \frac{3}{4}g_1^4 + \frac{3}{2}g_1^2g_2^2 - 3\lambda_1(3g_2^2 + g_1^2 - 4y_b^2\tilde{\Theta}) \right], \quad (\text{B11})$$

$$\beta(\lambda_2) = \frac{1}{16\pi^2} \left[12\lambda_2^2 + 4\lambda_3^2 + 4\lambda_3\lambda_4 + 2\lambda_4^2 + 2\lambda_5^2 - 12(y_t^4 + y_b^4\Theta) + \frac{9}{4}g_2^4 + \frac{3}{4}g_1^4 + \frac{3}{2}g_1^2g_2^2 - 3\lambda_2(3g_2^2 + \lambda_2g_1^2 - 4y_t^2 - 4y_b^2\Theta) \right], \quad (\text{B12})$$

$$\beta(\lambda_3) = \frac{1}{16\pi^2} \left[2(\lambda_1 + \lambda_2)(3\lambda_3 + \lambda_4) + 4\lambda_3^2 + 2\lambda_4^2 + 2\lambda_5^2 - 12y_t^2y_b^2\tilde{\Theta} + \frac{9}{4}g_2^4 + \frac{3}{4}g_1^4 - \frac{3}{2}g_1^2g_2^2 - 3\lambda_3(g_2^2 + g_1^2 - 2y_t^2 - 2y_b^2) \right], \quad (\text{B13})$$

$$\beta(\lambda_4) = \frac{1}{16\pi^2} \left[2\lambda_4(\lambda_1 + \lambda_2 + 4\lambda_3 + 2\lambda_4) + 8\lambda_5^2 + 12y_t^2y_b^2\tilde{\Theta} + 3g_2^2g_1^2 - 3\lambda_4(3g_2^2 + g_1^2 - 2y_t^2 - 2y_b^2) \right], \quad (\text{B14})$$

$$\beta(\lambda_5) = \frac{1}{16\pi^2} \left[2\lambda_5(\lambda_1 + \lambda_2 + 4\lambda_3 + 6\lambda_4) - 3\lambda_5(3g_2^2 + g_1^2 - 2y_t^2 - 2y_b^2) \right], \quad (\text{B15})$$

where

$$\Theta = 1(0) \quad \text{for Type-I, X (Type-II, Y)}, \quad (\text{B16})$$

$$\tilde{\Theta} = 0(1) \quad \text{for Type-I, X (Type-II, Y)}. \quad (\text{B17})$$

In the GM model, we obtain [22]

$$\beta(g_3) = \frac{g_3^3}{16\pi^2}(-7), \quad \beta(g_2) = \frac{g_2^3}{16\pi^2} \left(-\frac{11}{6} \right), \quad \beta(g_1) = \frac{g_1^3}{16\pi^2} \frac{47}{6}, \quad (\text{B18})$$

$$\beta(y_t) = \frac{1}{16\pi^2} \left[\frac{9}{2}y_t^3 + \frac{3}{2}y_b^3 - y_t \left(8g_3^2 + \frac{9}{4}g_2^2 + \frac{17}{12}g_1^2 \right) \right], \quad (\text{B19})$$

$$\beta(y_b) = \frac{1}{16\pi^2} \left[\frac{9}{2}y_b^3 + \frac{3}{2}y_t^3 - y_b \left(8g_3^2 + \frac{9}{4}g_2^2 + \frac{5}{12}g_1^2 \right) \right], \quad (\text{B20})$$

$$\beta(\lambda) = \frac{1}{16\pi^2} \left[\frac{3}{8} (3g_2^4 + 2g_2^2g_1^2 + g_1^4) + 24\lambda^2 - 6(y_t^4 + y_b^4) + 3\sigma_1^2 + 3\sigma_1\sigma_2 + \frac{5\sigma_2^2}{4} + 6\sigma_3^2 + 2\sigma_4^2 - 3\lambda(g_1^2 + 3g_2^2 - 4y_t^2 - 4y_b^2) \right], \quad (\text{B21})$$

$$\beta(\rho_1) = \frac{1}{16\pi^2} \left[15g_2^4 - 12g_1^2g_2^2 + 6g_1^4 + 28\rho_1^2 + 24\rho_1\rho_2 + 6\rho_2^2 + 6\rho_4^2 + 4\rho_4\rho_5 + 3\rho_5^2 + 2\sigma_1^2 + 2\sigma_1\sigma_2 - 12\rho_1(g_1^2 + 2g_2^2) \right], \quad (\text{B22})$$

$$\beta(\rho_2) = \frac{1}{16\pi^2} \left[24g_1^2g_2^2 - 6g_2^4 + 24\rho_1\rho_2 + 18\rho_2^2 - 2\rho_5^2 + \sigma_2^2 - 12\rho_2(2g_2^2 + g_1^2) \right], \quad (\text{B23})$$

$$\beta(\rho_3) = \frac{1}{16\pi^2} 2 (3g_2^4 + 22\rho_3^2 + 3\rho_4^2 + 2\rho_4\rho_5 + \rho_5^2 + 2\sigma_3^2 - 12g_2^2\rho_3), \quad (\text{B24})$$

$$\beta(\rho_4) = \frac{1}{16\pi^2} 2 \left[3g_2^4 + \rho_4 (8\rho_1 + 6\rho_2 + 10\rho_3 + 4\rho_4) + 2\rho_5(\rho_1 + \rho_2 + \rho_3) + \rho_5^2 + 2\sigma_1\sigma_3 + \sigma_2\sigma_3 + \sigma_4^2 - 3\rho_4(g_1^2 + 4g_2^2) \right], \quad (\text{B25})$$

$$\beta(\rho_5) = \frac{1}{16\pi^2} 2 \left[3g_2^4 + \rho_5 (2\rho_1 + 4\rho_3 + 8\rho_4 + 5\rho_5) - \sigma_4^2 - 3\rho_5(4g_2^2 + g_1^2) \right], \quad (\text{B26})$$

$$\beta(\sigma_1) = \frac{1}{16\pi^2} \left[3g_1^4 - 6g_1^2g_2^2 + 6g_2^4 + 2\sigma_1 (6\lambda + 8\rho_1 + 6\rho_2 + 2\sigma_1) + 2\sigma_2(2\lambda + 3\rho_1 + \rho_2) + 2 (6\rho_4\sigma_3 + 2\rho_5\sigma_3 + \sigma_4^2) + \sigma_2^2 - \frac{3}{2}\sigma_1(5g_1^2 + 11g_2^2 - 4y_t^2 - 4y_b^2) \right], \quad (\text{B27})$$

$$\beta(\sigma_2) = \frac{1}{16\pi^2} \left[12g_1^2g_2^2 + 4\sigma_2[\lambda + \rho_1 + 2(\rho_2 + \sigma_1) + \sigma_2] + 4\sigma_4^2 - \frac{3}{2}\sigma_2(5g_1^2 + 11g_2^2 - 4y_t^2 - 4y_b^2) \right], \quad (\text{B28})$$

$$\beta(\sigma_3) = \frac{1}{16\pi^2} \left[3g_2^4 + 2\sigma_3 (6\lambda + 10\rho_3 + 4\sigma_3) + (3\rho_4 + \rho_5)(2\sigma_1 + \sigma_2) + 4\sigma_4^2 - \frac{3}{2}\sigma_3(g_1^2 + 11g_2^2 - 4y_t^2 - 4y_b^2) \right], \quad (\text{B29})$$

$$\beta(\sigma_4) = \frac{1}{16\pi^2} \frac{\sigma_4}{2} \left[4(2\lambda + 2\rho_4 - \rho_5 + 2\sigma_1 + 2\sigma_2 + 4\sigma_3) - 3(3g_1^2 + 11g_2^2 - 4y_t^2 - 4y_b^2) \right]. \quad (\text{B30})$$

Appendix C: Contributions to the S, T parameters

In this section, we present the analytic expressions for the oblique S and T parameters in the extended Higgs sector models considered. Because we are interested in the NP contribution to these parameters, we define the differences as $\Delta S = S_{\text{NP}} - S_{\text{SM}}$ and $\Delta T = T_{\text{NP}} - T_{\text{SM}}$.

Let us start with the 2HDM within which the ΔS and ΔT parameters have the following

expressions:

$$\Delta S = \frac{1}{4\pi} \left\{ -F'(m_Z^2; m_{H^\pm}, m_{H^\pm}) + s_{\beta-\alpha}^2 F'(m_Z^2; m_H, m_A) \right. \\ \left. + c_{\beta-\alpha}^2 [F'(m_Z^2; m_h, m_A) - G'(m_Z^2; m_h, m_Z) + G'(m_Z^2; m_H, m_Z)] \right\}, \quad (\text{C1})$$

$$\Delta T = \frac{1}{4\pi e^2 v^2} \left\{ F(0; m_{H^\pm}, m_A) + s_{\beta-\alpha}^2 [F(0; m_{H^\pm}, m_H) - F(0; m_A, m_H)] \right. \\ \left. + c_{\beta-\alpha}^2 [F(0; m_{H^\pm}, m_h) - F(0; m_A, m_h)] \right. \\ \left. - G(0; m_h, m_W) + G(0; m_H, m_W) + G(0; m_h, m_Z) - G(0; m_H, m_Z) \right\}. \quad (\text{C2})$$

The loop functions are given by

$$F(p^2, m_1, m_2) = \int_0^1 dx [(2x-1)(m_1^2 - m_2^2) + p^2(2x-1)^2] \ln \Delta_B, \quad (\text{C3})$$

$$G(p^2, m_1, m_2) = \int_0^1 dx [(2x-1)m_1^2 - (2x-5)m_2^2 + p^2(2x-1)^2] \ln \Delta_B, \quad (\text{C4})$$

where $e^2 = 4\pi\alpha_{\text{em}}$ and

$$\Delta_B = -x(1-x)p^2 + xm_1^2 + (1-x)m_2^2, \quad (\text{C5})$$

$$F'(m_V^2; m_1, m_2) = [F(m_V^2; m_1, m_2) - F(0; m_1, m_2)]/m_V^2, \quad (\text{C6})$$

$$G'(m_V^2; m_1, m_2) = [G(m_V^2; m_1, m_2) - G(0; m_1, m_2)]/m_V^2. \quad (\text{C7})$$

In the HSM, the expressions are simpler:

$$\Delta S = \frac{s_\alpha^2}{4\pi} [G'(m_Z^2; m_H, m_Z) - G'(m_Z^2; m_h, m_Z)], \quad (\text{C8})$$

$$\Delta T = \frac{s_\alpha^2}{4\pi e^2 v^2} [G(0; m_H, m_W) - G(0; m_h, m_W) + G(0; m_h, m_Z) - G(0; m_H, m_Z)]. \quad (\text{C9})$$

In the GM model, we need a special treatment for the calculation of the T parameter. In fact, in this model an additional counter term δT appears due to the fact that the kinetic term is described by four independent quantities, namely g_1 , g_2 , v and ρ . We are here imposing $\rho = 1$ at the tree level by taking the two triplet VEVs to be the same. This means that the T parameter is not predictable in the GM model. We can indeed take any value of δT by setting a suitable renormalization condition. In our numerical evaluation, we simply set δT so as to satisfy $\Delta T = 0$ [44, 45].

The ΔS parameter in the GM model is given by:

$$\Delta S = \frac{1}{4\pi} \left\{ -5F'(m_Z^2; m_{H_5}, m_{H_5}) - F'(m_Z^2; m_{H_3}, m_{H_3}) \right. \quad (\text{C10})$$

$$\begin{aligned} & + \frac{10s_\beta^2}{3}F(m_Z^2, m_{H_5}, m_{H_3}) + 2c_\beta^2G'(m_Z^2, m_{H_5}, m_W) + \frac{4c_\beta^2}{3}G'(m_Z^2, m_{H_5}, m_Z) \\ & + \left(s_\alpha c_\beta - \frac{2}{3}\sqrt{6}c_\alpha s_\beta \right)^2 F'(m_Z^2, m_{H_3}, m_{H_1}) + \left(c_\alpha c_\beta + \frac{2}{3}\sqrt{6}s_\alpha s_\beta \right)^2 F'(m_Z^2, m_{H_3}, m_h) \\ & + \left(s_\alpha s_\beta + \frac{2}{3}\sqrt{6}c_\alpha c_\beta \right)^2 G'(m_Z^2, m_{H_1}, m_Z) + \left[\left(s_\beta c_\alpha - \frac{2}{3}\sqrt{6}c_\beta s_\alpha \right)^2 - 1 \right] G'(m_Z^2, m_h, m_Z) \left. \right\}. \end{aligned} \quad (\text{C11})$$

Appendix D: General potential in the GM model

The most general scalar potential, not custodial symmetric, in the GM model is given by [22]:

$$\begin{aligned} V(\Phi, \chi, \xi)_{\text{GM}} &= m_\Phi^2(\Phi^\dagger\Phi) + m_\chi^2\text{tr}(\chi^\dagger\chi) + m_\xi^2\text{tr}(\xi^2) \\ &+ \bar{\mu}_1\Phi^\dagger\xi\Phi + \bar{\mu}_2[\Phi^T(i\tau_2)\chi^\dagger\Phi + \text{h.c.}] + \bar{\mu}_3\text{tr}(\chi^\dagger\chi\xi) + \lambda(\Phi^\dagger\Phi)^2 \\ &+ \rho_1[\text{tr}(\chi^\dagger\chi)]^2 + \rho_2\text{tr}(\chi^\dagger\chi\chi^\dagger\chi) + \rho_3\text{tr}(\xi^4) + \rho_4\text{tr}(\chi^\dagger\chi)\text{tr}(\xi^2) + \rho_5\text{tr}(\chi^\dagger\xi)\text{tr}(\xi\chi) \\ &+ \sigma_1\text{tr}(\chi^\dagger\chi)\Phi^\dagger\Phi + \sigma_2\Phi^\dagger\chi\chi^\dagger\Phi + \sigma_3\text{tr}(\xi^2)\Phi^\dagger\Phi + \sigma_4(\Phi^\dagger\chi\xi\Phi^c + \text{h.c.}), \end{aligned} \quad (\text{D1})$$

where $\bar{\mu}_2$ and σ_4 are complex in general, but we here assume them real for simplicity. The doublet Φ and the triplet χ and ξ fields are parameterized as

$$\Phi = \begin{pmatrix} \phi^+ \\ \phi^0 \end{pmatrix}, \quad \chi = \begin{pmatrix} \frac{\chi^+}{\sqrt{2}} & -\chi^{++} \\ \chi^0 & -\frac{\chi^+}{\sqrt{2}} \end{pmatrix}, \quad \xi = \begin{pmatrix} \frac{\xi^0}{\sqrt{2}} & -\xi^+ \\ -\xi^- & -\frac{\xi^0}{\sqrt{2}} \end{pmatrix}, \quad (\text{D2})$$

where the neutral components are expressed by

$$\phi^0 = \frac{1}{\sqrt{2}}(\phi_r + v_\phi + i\phi_i), \quad \chi^0 = \frac{1}{\sqrt{2}}(\chi_r + i\chi_i^0) + v_\chi, \quad \xi^0 = \xi_r + v_\xi. \quad (\text{D3})$$

By comparing the custodial symmetric potential given in Eq. (28) with the general one in Eq. (D1), we find the following relations:

$$\begin{aligned} m_\phi^2 &= 2m_\Phi^2, \quad m_\chi^2 = 2m_\Delta^2, \quad m_\xi^2 = m_\Delta^2, \quad \bar{\mu}_1 = -\frac{\mu_1}{\sqrt{2}}, \quad \bar{\mu}_2 = -\frac{\mu_1}{2}, \quad \bar{\mu}_3 = 6\sqrt{2}\mu_2, \\ \lambda &= 4\lambda_1, \quad \rho_1 = 4\lambda_2 + 6\lambda_3, \quad \rho_2 = -4\lambda_3, \quad \rho_3 = 2(\lambda_2 + \lambda_3), \quad \rho_4 = 4\lambda_2, \quad \rho_5 = 4\lambda_3, \\ \sigma_1 &= 4\lambda_4 - \lambda_5, \quad \sigma_2 = 2\lambda_5, \quad \sigma_3 = 2\lambda_4, \quad \sigma_4 = \sqrt{2}\lambda_5, \end{aligned} \quad (\text{D4})$$

which express the 16 parameters of the most general potential in terms of the 9 parameters defined in the custodial symmetric one.

-
- [1] G. Aad *et al.* [ATLAS and CMS Collaborations], JHEP **1608**, 045 (2016) [arXiv:1606.02266 [hep-ex]].
 - [2] G. C. Branco, P. M. Ferreira, L. Lavoura, M. N. Rebelo, M. Sher and J. P. Silva, Phys. Rept. **516**, 1 (2012), arXiv:1106.0034 [hep-ph].
 - [3] H. Georgi and M. Machacek, Nucl. Phys. B **262**, 463 (1985).
 - [4] M. S. Chanowitz and M. Golden, Phys. Lett. B **165**, 105 (1985).
 - [5] M. Gonderinger, Y. Li, H. Patel and M. J. Ramsey-Musolf, JHEP **1001**, 053 (2010) [arXiv:0910.3167 [hep-ph]].
 - [6] T. P. Cheng and L. F. Li, Phys. Rev. D **22**, 2860 (1980);
J. Schechter and J. W. F. Valle, Phys. Rev. D **22**, 2227 (1980);
G. Lazarides, Q. Shafi and C. Wetterich, Nucl. Phys. B **181**, 287 (1981);
R. N. Mohapatra and G. Senjanovic, Phys. Rev. D **23**, 165 (1981);
M. Magg and C. Wetterich, Phys. Lett. B **94**, 61 (1980).
 - [7] [ATLAS Collaboration], arXiv:1307.7292 [hep-ex].
 - [8] [CMS Collaboration], arXiv:1307.7135.
 - [9] K. Fujii *et al.*, arXiv:1506.05992 [hep-ex].
 - [10] B. W. Lee, C. Quigg and H. B. Thacker, Phys. Rev. D **16**, 1519 (1977).
 - [11] I. F. Ginzburg and I. P. Ivanov, Phys. Rev. D **72**, 115010 (2005).
 - [12] S. Kanemura and K. Yagyu, Phys. Lett. B **751**, 289 (2015) [arXiv:1509.06060 [hep-ph]].
 - [13] S. Kanemura, T. Kubota and E. Takasugi, Phys. Lett. B **313**, 155 (1993).
 - [14] A. G. Akeroyd, A. Arhrib and E. M. Naimi, Phys. Lett. B **490**, 119 (2000). [arXiv:hep-ph/0006035].
 - [15] C. Y. Chen, S. Dawson and I. M. Lewis, Phys. Rev. D **91**, no. 3, 035015 (2015), [arXiv:1410.5488 [hep-ph]].
 - [16] S. Kanemura, M. Kikuchi and K. Yagyu, Nucl. Phys. B **917**, 154 (2017) [arXiv:1608.01582 [hep-ph]].
 - [17] S. L. Glashow and S. Weinberg, Phys. Rev. D **15**, 1958 (1977).

- [18] S. Davidson and H. E. Haber, Phys. Rev. D **72**, 035004 (2005) [Phys. Rev. D **72**, 099902 (2005)] [hep-ph/0504050].
- [19] V. D. Barger, J. L. Hewett and R. J. N. Phillips, Phys. Rev. D **41**, 3421 (1990).
- [20] Y. Grossman, Nucl. Phys. B **426**, 355 (1994).
- [21] M. Aoki, S. Kanemura, K. Tsumura and K. Yagyu, Phys. Rev. D **80**, 015017 (2009) [arXiv:0902.4665 [hep-ph]].
- [22] S. Blasi, S. De Curtis and K. Yagyu, Phys. Rev. D **96** (2017) no.1, 015001 [arXiv:1704.08512 [hep-ph]].
- [23] M. E. Peskin and T. Takeuchi, Phys. Rev. Lett. **65**, 964 (1990); Phys. Rev. D **46**, 381 (1992).
- [24] M. Baak *et al.*, Eur. Phys. J. C **72**, 2205 (2012) [arXiv:1209.2716 [hep-ph]].
- [25] F. Mahmoudi and O. Stal, Phys. Rev. D **81**, 035016 (2010) [arXiv:0907.1791 [hep-ph]].
- [26] T. Enomoto and R. Watanabe, JHEP **1605**, 002 (2016) [arXiv:1511.05066 [hep-ph]].
- [27] S. Kanemura, K. Tsumura, K. Yagyu and H. Yokoya, Phys. Rev. D **90**, no. 7, 075001 (2014) [arXiv:1406.3294 [hep-ph]].
- [28] S. Kanemura, H. Yokoya and Y. J. Zheng, Nucl. Phys. B **886**, 524 (2014) [arXiv:1404.5835 [hep-ph]].
- [29] The ATLAS collaboration [ATLAS Collaboration], ATLAS-CONF-2016-089.
- [30] G. Aad *et al.* [ATLAS Collaboration], JHEP **1508**, 148 (2015) [arXiv:1505.07018 [hep-ex]].
- [31] G. Aad *et al.* [ATLAS Collaboration], Phys. Rev. D **92**, 092004 (2015) [arXiv:1509.04670 [hep-ex]].
- [32] G. Aad *et al.* [ATLAS Collaboration], Eur. Phys. J. C **76**, no. 1, 45 (2016) [arXiv:1507.05930 [hep-ex]].
- [33] G. Aad *et al.* [ATLAS Collaboration], Phys. Lett. B **744**, 163 (2015) [arXiv:1502.04478 [hep-ex]].
- [34] G. Aad *et al.* [ATLAS Collaboration], Eur. Phys. J. C **76** (2016) no.1, 6 [arXiv:1507.04548 [hep-ex]].
- [35] S. Moretti, R. Santos and P. Sharma, Phys. Lett. B **760**, 697 (2016) [arXiv:1604.04965 [hep-ph]].
- [36] A. M. Sirunyan *et al.* [CMS Collaboration], arXiv:1705.02942 [hep-ex].
- [37] V. Khachatryan *et al.* [CMS Collaboration], Phys. Rev. Lett. **114**, no. 5, 051801 (2015) [arXiv:1410.6315 [hep-ex]].

- [38] S. Dawson, A. Gritsan, H. Logan, J. Qian, C. Tully, R. Van Kooten, A. Ajaib and A. Anastassov *et al.*, “Working Group Report: Higgs Boson,” arXiv:1310.8361 [hep-ex].
- [39] G. Cynolter, E. Lendvai and G. Pocsik, Acta Phys. Polon. B **36**, 827 (2005) [hep-ph/0410102].
- [40] S. Kanemura, M. Kikuchi and K. Yagyu, Nucl. Phys. B **907**, 286 (2016) [arXiv:1511.06211 [hep-ph]].
- [41] M. Aoki and S. Kanemura, Phys. Rev. D **77**, no. 9, 095009 (2008) Erratum: [Phys. Rev. D **89**, no. 5, 059902 (2014)] [arXiv:0712.4053 [hep-ph]].
- [42] K. Hartling, K. Kumar and H. E. Logan, Phys. Rev. D **90**, no. 1, 015007 (2014) [arXiv:1404.2640 [hep-ph]].
- [43] L. Basso, O. Fischer and J. J. van Der Bij, Phys. Lett. B **730**, 326 (2014) [arXiv:1309.6086 [hep-ph]].
- [44] J. F. Gunion, R. Vega and J. Wudka, Phys. Rev. D **43**, 2322 (1991).
- [45] C. W. Chiang, A. L. Kuo and K. Yagyu, arXiv:1707.04176 [hep-ph].